Estimation of Stratospheric Intrusions During Indian Cyclones

Chaitri Roy, A. Ravishankara, Paul Newman, Liji David, Suvarna Fadnavis, Sagar Rathod, Leslie Lait, R. Krishnan, Hannah Clark, Bastien Sauvage

JGR Atmospheres

RESEARCH ARTICLE
10.1029/2022JD037519

Estimation of Stratospheric Intrusions During Indian Cyclones

Chaitri Roy[1,2,3], A. R. Ravishankara[3,4], Paul A. Newman[5], Liji M. David[3,4,6], Suvarna Fadnavis[1,2], Sagar D. Rathod[3,7], Leslie Lait[8], R. Krishnan[1,2], Hannah Clark[9], and Bastien Sauvage[10]

[1]Centre for Climate Change Research, Indian Institute of Tropical Meteorology, Ministry of Earth Sciences, Pune, India, [2]Savitribai Phule Pune University, Pune, India, [3]Department of Atmospheric Science, Colorado State University, Fort Collins, CO, USA, [4]Department of Chemistry, Colorado State University, Fort Collins, CO, USA, [5]NASA Goddard Space Flight Centre, Greenbelt, MD, USA, [6]Bingham Research Center, Utah State University, Vernal, UT, USA, [7]La Follette School of Public Affairs, University of Wisconsin, Madison, WI, USA, [8]Science Systems & Applications Inc., Lanham, MD, USA, [9]IAGOS-AISBL, Brussels, Belgium, [10]Laboratoire d'Aérologie, Université de Toulouse, CNRS, Université Paul Sabatier Toulouse III, Toulouse, France

Abstract Deep convection associated with tropical cyclones leads to stratosphere-troposphere exchange (STE), which affects the upper-tropospheric ozone concentrations in the vicinity of the cyclones. This study estimates the ozone enhancements over India due to the North Indian Ocean (NIO) cyclones-driven STE. Indicators such as stratospheric fraction and potential vorticity calculated using the reanalysis data sets suggest that roughly 70% of the cyclones show anomalously high stratospheric intrusions. Aircraft observations over different locations across India also show elevated ozone concentrations in the mid-to-upper troposphere on cyclone days. Further, ozone and stratospheric ozone tracer concentrations from Goddard Earth Observing System-Chemistry simulations and the Copernicus Atmosphere Monitoring Service reanalysis data sets show up to 40 ppb of excess upper tropospheric ozone over India, of which stratospheric ozone accounts for roughly 60%. Stratospheric intrusion due to the Bay of Bengal and the Arabian Sea cyclones affected the upper tropospheric ozone amounts over North and South India, respectively. The stratospheric ozone was observed to propagate downwards into the troposphere, often reaching ~600 hPa and, in some cases, even the surface.

Plain Language Summary This study estimates the increase in the amount of ozone in the upper half of the lower atmosphere ("upper troposphere") during the North Indian Ocean (NIO) cyclones. Ozone in the upper atmosphere ("stratosphere") protects the Earth from harmful ultraviolet radiation but affects human and ecosystem health when present in the lower atmosphere ("troposphere"). Generally, the ozone in the lower atmosphere occurs due to chemical reactions of gases and sometimes due to the transport from the ozone-rich upper atmosphere. However, there is a barrier between the upper and the lower atmospheres, also known as the tropopause. Using observations and atmospheric models, we study the penetration of ozone from the upper atmosphere to the lower atmosphere, during the NIO cyclones which disturb the separation barrier. We studied 20 cyclones and found that they disturb the barrier between the upper and the lower atmosphere significantly over India and a large amount of ozone moves between them, so much so that it almost doubles the ozone concentration in the upper half of the lower atmosphere. A warmer world in the future could lead to more cyclones which could increase ozone in the lower atmosphere.

Key Points:

- Stratosphere-troposphere exchange (STE) over India due to the North Indian Ocean cyclones is studied using reanalysis data and model output
- Enhanced stratospheric airmass (~20%) and ozone (~40 ppb) were evident in the upper troposphere and lower stratosphere
- STE due to the Bay of Bengal and Arabian Sea cyclones influence ozone amplification over northern and southern India, respectively

Supporting Information:

Supporting Information may be found in the online version of this article.

Correspondence to:

C. Roy,
chaitri.cat@tropmet.res.in

Citation:

Roy, C., Ravishankara, A. R., Newman, P. A., David, L. M., Fadnavis, S., Rathod, S. D., et al. (2023). Estimation of stratospheric intrusions during Indian cyclones. *Journal of Geophysical Research: Atmospheres*, *128*, e2022JD037519. https://doi.org/10.1029/2022JD037519

Received 19 JUL 2022
Accepted 27 DEC 2022

Author Contributions:

Conceptualization: Chaitri Roy, A. R. Ravishankara, Paul A. Newman
Data curation: Chaitri Roy, Liji M. David, Sagar D. Rathod, Leslie Lait, Hannah Clark, Bastien Sauvage
Formal analysis: Chaitri Roy, Sagar D. Rathod
Funding acquisition: A. R. Ravishankara
Investigation: Chaitri Roy, A. R. Ravishankara, Paul A. Newman, Liji M. David, Suvarna Fadnavis, Sagar D. Rathod, Leslie Lait, R. Krishnan, Bastien Sauvage
Methodology: Chaitri Roy, A. R. Ravishankara, Paul A. Newman
Resources: Paul A. Newman, Liji M. David, Hannah Clark

1. Introduction

Ozone abundance near the tropopause is controlled by photochemistry, large-scale transport processes such as the Brewer-Dobson circulation, and meteorological transport phenomenon typically referred to as stratosphere-troposphere exchange (STE). While the Brewer-Dobson circulation is a global large-scale mass circulation, STE is a synoptic-scale bi-directional exchange of air between the stratosphere and the troposphere across the tropopause. More commonly, STE is referred to as a unidirectional exchange from the stratosphere to the troposphere (Stohl, 2001; Wernli & Bourqui, 2002), and is associated with episodic events (Appenzeller & Davies, 1992). It has been chiefly observed during events such as Rossby wave breaking (RWB) in the vicinity of sub-tropical westerly jets, breaking of gravity waves, and episodes of monsoon breaks (Lamarque et al., 1996; Samanta et al., 2016; Sprenger et al., 2003; Zachariasse et al., 2001). Tropical cyclones lead to large amounts of stratospheric air displacement across the tropopause into the troposphere (Baray et al., 1999; Das, 2009; Zhan & Wang, 2012) and are another driver of STE. They are the focus of this paper.

Supervision: A. R. Ravishankara, Paul A. Newman, Suvarna Fadnavis, R. Krishnan
Visualization: Chaitri Roy, A. R. Ravishankara, Paul A. Newman, Sagar D. Rathod
Writing – original draft: Chaitri Roy, A. R. Ravishankara, Paul A. Newman, Liji M. David, Suvarna Fadnavis, Sagar D. Rathod, Leslie Lait, R. Krishnan, Hannah Clark, Bastien Sauvage
Writing – review & editing: Chaitri Roy, A. R. Ravishankara, Paul A. Newman, Liji M. David, Suvarna Fadnavis, Sagar D. Rathod, Leslie Lait, R. Krishnan, Hannah Clark, Bastien Sauvage

The intrusion of stratospheric air has several consequences. It can enhance the ozone concentration near the tropopause, which may alter the global radiative budget and affect climate change (Roy et al., 2017, 2020). It is important for determining the tropospheric ozone budget (Voulgarakis et al., 2010; Wild, 2007), and can also impact the abundance of surface ozone for air quality (Langford et al., 2018; Lin et al., 2012; Roelofs & Lelieveld, 1997; L. Zhang et al., 2020). Therefore understanding the exchange processes that occur in the vicinity of the tropopause and quantifying this exchange is of broad interest.

Tropical cyclones are synoptic-scale deep convective systems with a horizontal extent of hundreds of kilometers and lifespans of days to weeks. They provide favorable pathways for the convective transport of water-vapor-rich and ozone-poor tropospheric air into the upper troposphere and lower stratosphere (UTLS) (Leclair De Bellevue et al., 2007; Ray & Rosenlof, 2007; Romps & Kuang, 2009). High sea surface temperature (SST; greater than 26°C), high mid-tropospheric humidity, and low wind shear are important factors responsible for the genesis of tropical cyclones (Gray, 1968). Tropical cyclones draw their energy primarily from evaporation at the warm ocean surface (Riehl, 1950), and their intensity and lifetime are dominated mainly by the ocean temperature distribution (Kaplan & DeMaria, 2003). Rapid episodes of overshooting convection associated with tropical cyclones weaken the tropopause stability and lead to the exchange of airmass between troposphere and stratosphere (Baray et al., 1999; Das, 2009; Das et al., 2011; Jiang et al., 2015; Merrill, 1988; Venkat Ratnam et al., 2016; Zhan & Wang, 2012). Other factors, such as the gravity waves breaking and wind shear generated turbulence during tropical cyclones, also influence STE (Langford et al., 1996; Shapiro, 1976).

Several authors have highlighted the role of cyclones formed over different ocean basins in inducing STE and their subsequent influence on the upper tropospheric ozone and water vapor contents. For instance, 50% of the total STE events have been observed to occur in the vicinity of the North Atlantic cyclones, whose intensity were primarily determined by the cyclones' strength. Further, it is understood that STE peaks on the day when a cyclone attains its maximum intensity (Reutter et al., 2015). Upper tropospheric moistening in the vicinity of the Atlantic or the Pacific cyclones has been observed from satellites (Ray & Rosenlof, 2007; Romps & Kuang, 2009). The upper tropospheric water vapor concentrations near these cyclones have also been reported to increase by 50% above their monthly average concentration (Ray & Rosenlof, 2007). Ozone mole fractions as high as 300 ppb at 300 hPa have been reported during cyclone Marlene, which formed near Reunion Island and Mauritius (Baray et al., 1999). The dynamical mechanism of enhancing upper tropospheric ozone during cyclone Marlene has also been studied (Leclair De Bellevue et al., 2007). High mid-to-upper-tropospheric ozone and potential vorticity (PV) during tropical cyclones have been observed near Taipei, Taiwan, by In-service Aircraft for a Global Observing System (IAGOS; Roux et al., 2020).

India's long coastline includes the two North Indian Ocean (NIO) basins—the Arabian Sea (AS) to the west and the Bay of Bengal (BoB) to the east—with warm SSTs (28°C–30°C). They are breeding grounds for tropical cyclones during the pre-monsoon (May–June) and the post-monsoon (October–November) seasons (Deshpande et al., 2021; Mohapatra et al., 2014; Shaji et al., 2014). Several authors have highlighted the NIO cyclones' role in inducing cross-tropopause exchange of ozone and water vapor. Enhanced upper and lower tropospheric ozone concentrations (20–50 ppbv and 10–15 ppbv, respectively) over India have been observed during two NIO cyclones (Das et al., 2016a). Radar observations of stratospheric intrusion during a 2001 BoB cyclone have been reported (Das, 2009). Cross-tropopause mass fluxes during the NIO cyclones have been studied using satellite observations and Global Positioning System radio occultation (GPS-RO) measurements. The study also elaborated on the role of cyclones in determining the tropopause structure and concentrations of ozone and water vapor in the UTLS within a radius of 1,000 km of the cyclone center (Venkat Ratnam et al., 2016). Enhanced upper tropospheric ozone during two BoB cyclones has also been observed from Microwave Limb Sounder (MLS; Pathakoti et al., 2016). Further, cyclones' impacts on the tropical tropopause parameters have been assessed from Constellation Observing System for Meteorology, Ionosphere, and Climate (COSMIC) GPS-RO temperature profiles (Ravindra Babu et al., 2015).

Cyclone-driven stratospheric intrusions have a short timescale of a few days. Therefore, studying them would require data sets with very high temporal, spatial, and vertical resolution. However, most previous work on the NIO cyclones-driven stratospheric intrusion relied either on in situ observations which have less spatial coverage, or on satellite observations which have low vertical resolution. In this study, we examine the spatial and vertical distributions of the indicators of stratospheric intrusion (such as ozone abundance and PV) during the NIO cyclones. We estimate the excess upper tropospheric ozone from cyclones using aircraft observations, daily gridded reanalysis data sets, and chemistry transport model simulations. Stratospheric fraction (SF), a newly

developed proxy for stratospheric intrusion derived from ozone and water vapor concentrations, and stratospheric ozone tracer are used to substantiate the presence of stratospheric air in the upper troposphere. The paper is organized as follows: Section 2 describes data and methods; Sections 3 and 4 present results and discussion; and Section 5 lists our conclusions.

2. Data and Methods

2.1. Observational Data Sets

Ozone variability from the surface to the upper atmosphere can be ideally studied from data sets having very high vertical, temporal, and spatial resolution. Although in situ observations, such as ozonesondes and aircraft measurements, have a very high vertical resolution, their temporal resolution and spatial coverage remain poor. Since launching ozonesondes to measure vertical ozone profiles both in and near a cyclone is difficult, available data is minimal. Also, IAGOS aircraft observations depend on the specific aircraft at a particular sector and, thus, are highly sporadic. On the other hand, satellite observations provide more spatial coverage, but the vertical resolution is limited. Satellite measurements are obtained only a few times a day. Also, they have a daytime bias since many satellites measure back-scattered sunlight. In this study, we used the ascending and descending ozone profiles from IAGOS aircraft measurements at or near a few Indian airports when there was a NIO cyclone. We have only used satellite-derived cloud top temperatures (CTT) to understand the extent and intensity of the cyclones.

2.1.1. In Situ Observation From IAGOS Aircraft Data

IAGOS provides in situ ozone profiles from the surface up to 9–12 km near many airports across the globe. The instrument which measures ozone has a detection limit of 2 ppbv and a precision of 2% (Nédélec et al., 2015; Petzold et al., 2015). The IAGOS ozone profiles are almost unbiased to weather conditions (except for the specific aircraft operations due to weather). However, ozone profiles are not expected in the proximity of the cyclones. Therefore we use the profiles available at different airports across the Indian subcontinent (Delhi, Hyderabad, and Chennai) between 2007 and 2017, where we expect to see the impacts of stratospheric ozone intrusion due to the NIO cyclones. These observations do not occur precisely when the cyclone is over land but close enough in time and space to provide some information (IAGOS, 2013). In a similar study, Roux et al. (2020) used IAGOS profiles over Taipei to assess the impacts of cyclones (typhoons) formed over the Pacific on trace gases in the troposphere.

2.1.2. MODIS Satellite Data

The MODIS instruments are on-aboard the Terra and Aqua satellites (Boeke et al., 2016; Platnick et al., 2003), which orbit over a region in the morning (10:30 a.m. local) and the afternoon (01:30 p.m. local), respectively. The cloud top pressure is converted to cloud temperature through the National Center for Environmental Prediction Global Forecast System (Derber et al., 1991). We use the daily level-3 MODIS cloud top temperature derived from level-2 aerosols, water vapor, cloud, and atmospheric profile. MODIS Daily Global data product files containing data collected from the Terra and Aqua platforms are MOD08_D3 and MYD08_D3, respectively (Platnick et al., 2015).

2.2. Measures of Stratospheric Intrusion

We calculate the relative percentages of stratospheric and tropospheric air at different vertical levels based on ozone and water vapor concentrations from Modern-Era Retrospective Analysis for Research and Applications, Version 2 (MERRA-2) reanalysis. We also analyze PV on isentropic levels from European Centre for Medium-Range Weather Forecasts (ECMWF) Interim (ERA-Interim) reanalysis data, and ozone and stratospheric ozone tracer concentrations from Copernicus Atmosphere Monitoring Service (CAMS) reanalysis data. The reanalysis products combine observations with short-range forecasts using data assimilation and, therefore, provide a complete picture of weather and climate. These data sets have a high temporal, spatial as well as vertical resolution.

2.2.1. Stratospheric Fraction (SF)

The standard tropopause is commonly defined by the change in temperature lapse rate ($dT/dZ < 2°C\ km^{-1}$). Other definitions of stratosphere-troposphere separations near the tropopause are based on either ozone concentration

changes, called the ozoneopause (the vertical point where there is a large increase of ozone concentration), or water vapor concentration changes, called the hygropause (the altitude where water vapor levels sharply decrease with altitude). Since stratospheric air is typically characterized by high concentrations of ozone (>200 ppb) and low concentrations of water vapor (<100 ppm), the tropopause can also be thought of as the layer where there is a drastic change in tracer concentrations.

The ozone and water vapor tracer-tracer relationship can be used to examine the transition from the troposphere to the stratosphere semi-quantitatively. This relationship can also provide another definition of the "tropopause." This relationship is used to estimate the influence of the stratosphere on air found in the troposphere and vice-versa. The "SF" diagnostic is calculated using ozone concentrations and specific humidity from MERRA-2 assimilated observations. The region where ozone mixing ratios are above 1,000 ppb is considered to have 100% stratospheric air. In contrast, the region where water vapor mixing ratios were above 200 ppm is considered to have 0% stratospheric air. The SF is the fraction of the angle of the line in a plot of $\log_{10}O_3$ versus $\log_{10}H_2O$ drawn from an "origin" (set to be O_3 = 1,000 ppb and H_2O = 200 ppm or $\log_{10}O_3/\log_{10}H_2O$ = 2.3) to an angle of 90°. We express the SF as a percentage. This algorithm is however fairly insensitive to large changes of the "origin" point or for observation errors because it is estimated in log-log space. The use of the 1,000 ppb and 200 ppm values as 100% stratospheric and 100% tropospheric air, respectively, are conservative estimates for the stratosphere and troposphere, and are easily seen in a climatology of these atmospheric layers. An example of ozone versus water vapor plot from MERRA-2 (thinned arrays) for 15 March 2018 is shown in Figure S1 in Supporting Information S1. For a nominal value of 180 ppb of ozone and 20 ppm of water vapor, SF is 61% for our algorithm. Changing the algorithm "origin" values for ozone and water vapor creates an absolute value SF change, but the relative values remain unchanged, that is, the vertical and horizontal structural patterns of SF remain the same. Figure S1 in Supporting Information S1 also shows how a 25% error in the ozone and water assimilation values lead to only a small change in the SF value (black oval line).

2.2.2. MERRA-2 Reanalysis Data

MERRA-2 (Gelaro et al., 2017) is NASA's atmospheric reanalysis, produced using information from the modern satellites (Molod et al., 2015). This reanalysis product also assimilates Aura's Ozone Monitoring Instrument (OMI) total column ozone data and MLS ozone profiles since October 2004 (Wargan et al., 2017). MERRA-2 data sets are continuous and gridded (0.5° × 0.625° resolution, with 72 vertical levels from the surface to 0.01 hPa). In this study, we use ozone, specific humidity, and various other meteorological fields (GMAO, 2015).

2.2.3. ECMWF Reanalysis Data

The ECMWF reanalysis system combines observations with the forecast model data using a four-dimensional variational (4D-Var) data assimilation technique to produce output every 6 hr, reflecting the atmospheric state's evolution. ECMWF interim reanalysis data is archived on pressure and isentropic levels (ERA-Interim, 0.75° × 0.75° grid resolution, with 60 vertical levels from the surface to 0.1 hPa) (Dee et al., 2011; Uppala et al., 2005). Here, we use PV on isentropic levels, which is available (ERA-Interim, 2011).

2.2.4. CAMS Reanalysis Data

The CAMS reanalysis is a global data set of atmospheric composition, including chemical species, aerosols, and greenhouse gases. The data is produced by assimilating satellite retrievals of ozone, carbon monoxide (CO), nitrogen dioxide (NO_2), and aerosol optical depth into ECMWF's Integrated Forecast System using the 4DVar data assimilation technique. This assimilation is a continuous global gridded data set (0.75° × 0.75° resolution, with 60 hybrid sigma-pressure levels extending from surface to 1 hPa; Flemming et al., 2017, 2015). We use ozone and stratospheric ozone tracer data sets available between 2007 and 2017 (Inness et al., 2019).

2.3. Model Details and Simulation Setup

We use a global 3-D chemical transport model, Goddard Earth Observing System-Chemistry (GEOS-Chem) version 13.0.0 (2° × 2.5° resolution, with 47 eta vertical levels from the surface up to ∼80 km). The meteorology is from MERRA-2 reanalysis data. The model is configured using the Harvard NASA Emissions Component module (Keller et al., 2014). The anthropogenic NO, CO, SO_2, and nonbiogenic VOC emissions are from the Community Emissions Data System inventory (Hoesly et al., 2018). The biomass burning emissions are from the Global Fire Emissions Database version 4 (Giglio et al., 2013). The biogenic VOC emissions are from

Table 1
List of the North Indian Ocean Cyclones During 2007–2017

Serial number	Cyclone name	Cyclone intensity	Duration	Most intense day (Day 0)	Basin
1	Gonu	SuCS	1–7 June 2007	4 June 2007	AS
2	Sidr	ESCS	11–16 November 2007	15 November 2007	BoB
3	Nargis	ESCS	27 April to 3 May 2008	29 April 2008	BoB
4	Aila	SCS	23–26 May 2009	25 May 2009	BoB
5	Laila	SCS	17–21 May 2010	19 May 2010	BoB
6	Phet	VSCS	30 May to 7 June 2010	2 June 2010	AS
7	Giri	ESCS	20–23 October 2010	22 October 2010	BoB
8	Jal	SCS	1–8 November 2010	6 November 2010	BoB
9	Thane	VSCS	25–31 December 2011	28 December 2011	BoB
10	Phailin	ESCS	6–14 October 2013	11 October 2013	BoB
11	Helen	SCS	19–23 November 2013	20 November 2013	BoB
12	Leher	VSCS	23–28 November 2013	26 November 2013	BoB
13	Madi	VSCS	6–13 December 2013	8 December 2013	BoB
14	Hudhud	ESCS	7–14 October 2014	12 October 2014	BoB
15	Nilofar	ESCS	25–31 October 2014	28 October 2014	AS
16	Chapala	ESCS	28 October to 4 November 2015	30 October 2015	AS
17	Megh	ESCS	5–10 November 2015	8 November 2015	AS
18	Vardah	VSCS	6–13 December 2016	9 December 2016	BoB
19	Mora	SCS	28–31 May 2017	28 May 2017	BoB
20	Ockhi	VSCS	29 November to 6 December 2017	1 December 2017	AS

Note. SuCS, Super cyclonic storm; ESCS, Extremely severe cyclonic storm; VSCS, Very severe cyclonic storm; SCS, Severe cyclonic storm.

the Model of Emissions of Gases and Aerosols from Nature version 2.1 (Guenther et al., 2012). The Universal tropospheric-stratospheric Chemistry eXtension (UCX) mechanism is used for the STE of O_3 (Eastham et al., 2014).

Due to computational limitations, we only perform full chemistry simulations for 2007, 2009, 2013, and 2015. Each simulation is initialized with a 1 year spin-up. GEOS-Chem has been previously evaluated for ozone over the Indian subcontinent using long-term observations from satellite, ozonesonde, and aircraft (David et al., 2019). The tagged simulations are performed as in David and Ravishankara (2019), where ozone produced in the stratosphere is marked and subjected to the same chemical and dry deposition losses as those for the total ozone. The ozone production and loss rates are provided from the full chemistry simulations. The total daily ozone calculated from all the regions in the tagged ozone simulations equals the total ozone from the full chemistry simulation.

2.4. Overview of the NIO Cyclones

Tropical cyclones that originate over the NIO (between 45° and 100°E) are monitored by the India Meteorological Department (IMD), which uses a criterion of 3 min sustained wind speeds to determine the strength of a cyclonic storm, in contrast to the Saffir-Simpson Hurricane Scale, which uses a criterion of 1 min sustained wind speed to classify hurricanes. Classification of cyclonic systems over the NIO based on IMD's criteria is described in Table S1 in Supporting Information S1.

We study stratospheric intrusions during all the intense NIO cyclones (category 2 and above) between 2007 and 2017 (listed in Table 1). During this period, six cyclones formed over the AS, while 14 cyclones formed over the BoB. These cyclones were predominantly observed during pre-monsoon (May–June) and post-monsoon (October–November) seasons over the BoB and the AS. Since maximum STE has been previously observed during the mature phase, when a cyclone attained its maximum intensity (Reutter et al., 2015), STE was studied for the day a cyclone reached its peak intensity, which is termed as Day 0. The ozone or SF anomalies were

calculated from the difference between ozone or SF on Day 0 and the mean ozone or SF of the preceding week (Day -1 to Day -7) when we assume STE to be small. The choice of Day -1 to Day -7 for the "background" state to examine the changes due to cyclone is a compromise. First, the position of the cyclone changes significantly during these dates. Second, there could be some perturbations on Day -1, Day -2, etc., because the cyclone, though may not be as strong, still perturbs the dynamics. Third, going much further back than Day -7 may also be influenced other processes and not necessarily a good indicator of the "background" for the change during the cyclone. Further, we also observe that the ozone anomalies obtained from using either Day -8 to Day -14 or Day -1 to Day -7 as "background" do not show a qualitatively different picture (Figure S2 in Supporting Information S1). One could also use monthly averages during the past years when there were no cyclones for comparison. However, such a choice also has possible biases since there could be other processes contributing to the ozone changes as already mentioned. As we noted, there is no perfect "background" to use. Therefore, we have settled on the use of the week before the cyclone for this study.

3. Results

3.1. Location and Extent of the Cyclones

Intensities of tropical cyclones and hurricanes have been previously studied using CTT values (Dvorak, 1975; Luo et al., 2008; Velden et al., 2006; Vergados et al., 2014; Wong & Emanuel, 2007). The location and geographical extent of a hurricane or a cyclone can also be determined from the CTT. Figure 1 shows the CTT of four cyclones of different intensities formed over the NIO. The CTT for other cyclones included in this study are shown in Figure S3 in Supporting Information S1. On Day 0, the CTT values were below 200 K over the cyclonic regions, and the cyclones extended to ∼10° (latitude) ×10° (longitude). For reference, CTT during a tropical cyclone Nilofar has been previously reported to reach 180 K on the day of its maximum intensity (Bhutto et al., 2017). The cold point tropopause temperature over the tropics ranged between 180 and 200 K (Gettelman et al., 2010).

The knowledge of CTT provides an estimate of troposphere-stratosphere transport (Danielsen, 1993; Folkins & Martin, 2005). All the cyclones discussed in this study have a sufficiently low CTT on Day 0 to disturb the

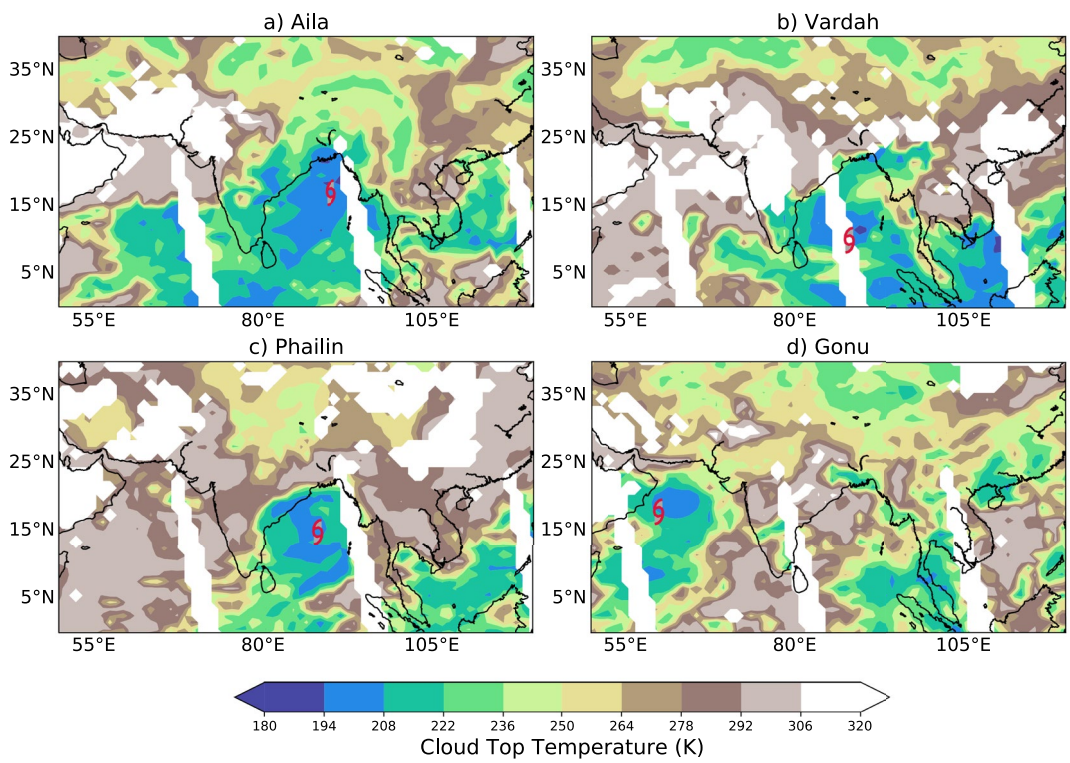

Figure 1. MODIS cloud top temperatures (K) on Day 0 for cyclones (a) Aila, (b) Vardah, (c) Phailin, and (d) Gonu. The red markers show cyclone locations.

tropopause and lead to cross-tropopause exchange. The tropical tropopause layer (TTL) is the region in the tropics which determines STE (Brewer, 1949; Gettelman & de F Forster, 2002). Tropical cyclones play a critical role in crossing the TTL and humidifying the stratosphere (Romps & Kuang, 2009). Upper tropospheric water vapor on Day 0 followed a similar distribution as CTT. On average, 1,000 ppm and 150 ppm water vapor were observed at 300 and 200 hPa, respectively, collocated over the regions of the cyclones (Figures S4–S5 in Supporting Information S1).

3.2. SF in the Upper Troposphere

SF in the upper troposphere can identify the exchange of material between the stratosphere and the troposphere and give a semi-quantitative estimate of the stratospheric air that comes into the troposphere during the NIO cyclones. We observe that on the days when there were no cyclones over the NIO, the 200 hPa SF was less than 10% over the Indian region (~5°–28°N), whereas it was more than 20% over the extra-tropical region (Figure S6 in Supporting Information S1). But on days when there was a cyclone over the NIO, the 200 hPa SF indicated a prominent meridional gradient over the Indian region, with high SF (greater than 50%) over central to northern India (above 15°N) and low SF (~10%–30%) over southern India (between 5° and 15°N; Figure S7 in Supporting Information S1). The 200 hPa SF anomalies on Day 0 of four cyclones can be seen in Figure 2. The SF anomalies of other cyclones included in this study are shown in Figure S8 in Supporting Information S1. Almost 75% of the cyclonic systems formed over the NIO show high SF anomalies (~10%–30%), especially over northern India (15°–28°N). SF anomalies over southern India remained below 10%. The north-eastern edge of the cyclone center shows negative SF anomalies (−10%) for more than half of the cyclones. This may be the region of maximum tropospheric outflow and divergence. We also notice a spatial variability in SF across the different cyclones. Such variability may be due to the location and strength of the cyclone, upper tropospheric tropical-extra-tropical interactions, or the interplay with various orographic features across India.

The dynamical tropopause, indicated by a solid white line corresponding to 2 PVU (1 PVU = 10^{-6} m^2 s^{-1} K kg^{-1}) (Holton et al., 1995; Hoskins et al., 1985; Thouret et al., 2006), is located at a higher altitude over the tropics compared to the extra-tropics (Figure S9 in Supporting Information S1). The lower tropopause height in the

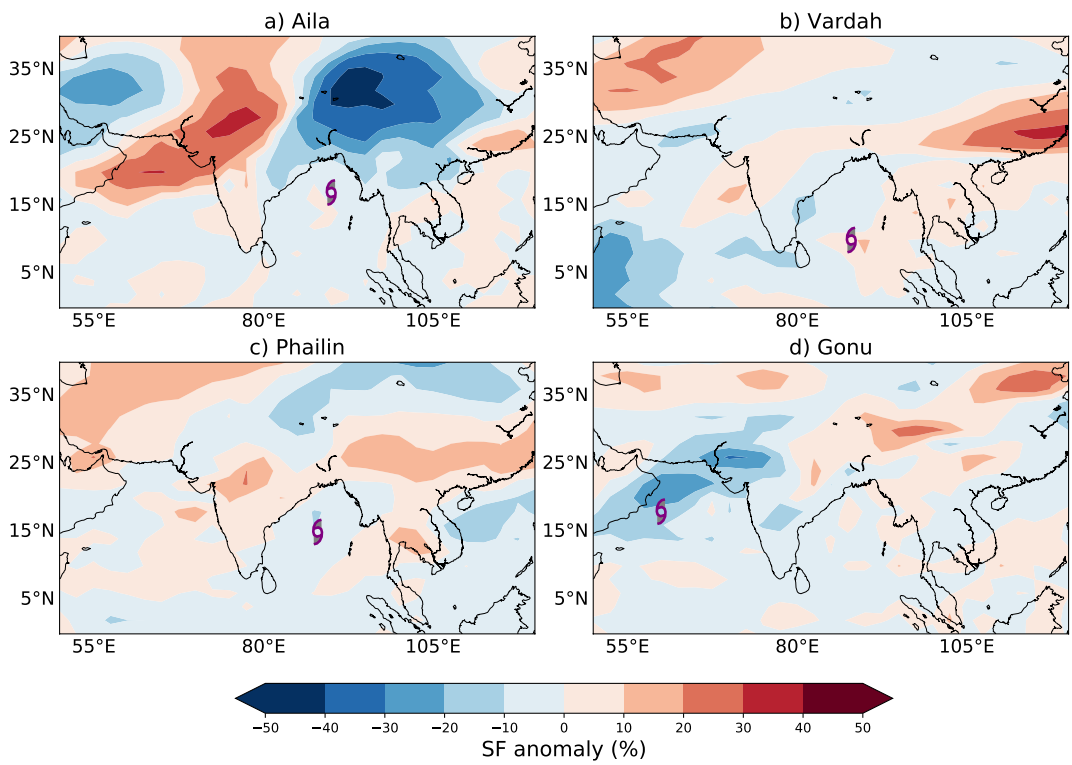

Figure 2. The distribution of the 200 hPa stratospheric fraction (SF) anomalies (%) on Day 0 for cyclones (a) Aila, (b) Vardah, (c) Phailin, and (d) Gonu. The purple markers show cyclone locations.

extra-tropics (north of the subtropical jet) results in the observed meridional gradient in SF in Figure S7 in Supporting Information S1. Nearly 40%–70% SF is present in the UTLS in both the latitudinal and longitudinal cross-sections of SF (Figures S9 and S10 in Supporting Information S1). Figure 3 shows the latitudinal cross-sections of SF anomaly for four cyclones. Other cyclones included in this study are shown in Figure S11 in Supporting Information S1. We observe a downward intrusion of excess SF (>15%) upto ∼300 hPa over northern India (15°–28°N) during ∼70% of the NIO cyclones. The meridional distribution of STE can be studied from the isentropic diagnostics (Appenzeller et al., 1996; Yang et al., 2016). We observe that the cross-tropopause transport of SF takes place along the 320–360 K isentropes. Maximum STE occurs along the boundary separating the tropics and the extra-tropics (∼30°N), where the core of the tropospheric jet stream was located (as seen from the wind contours in Figure 3 and Figure S11 in Supporting Information S1).

Longitudinal cross-sections of SF anomalies (averaged over 20°–35°N) show tropopause folding for 80% of the NIO cyclones (Figure 4 and Figure S12 in Supporting Information S1). Stratospheric intrusion over India via tropopause folding occurs through one or both sides of the cyclone center and reaches up to ∼500 hPa. Previous studies have noted that deep convective systems often disturb the tropopause structure, which leads to a strong downdraft in the vicinity of the tropopause (K. K. Kumar, 2006). The disturbance near the tropopause leads to

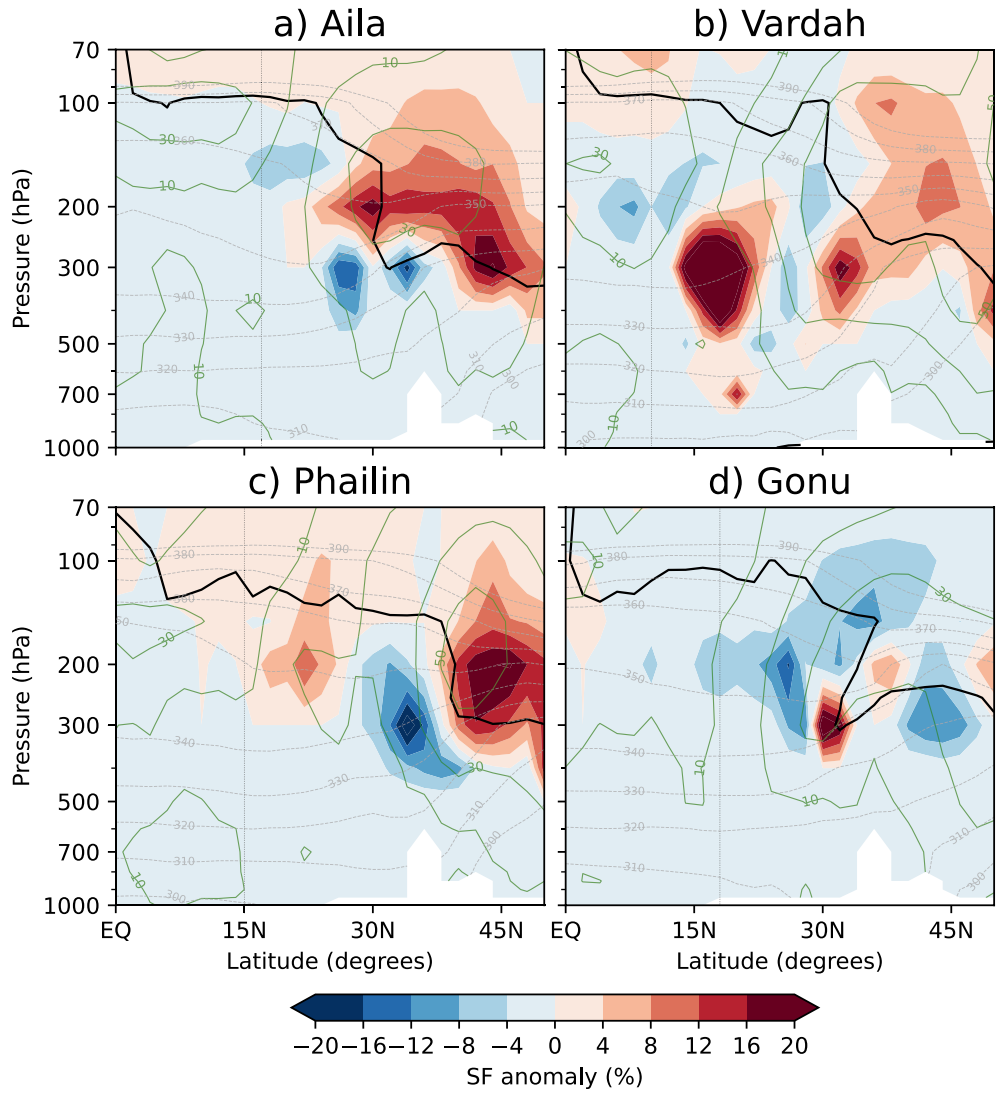

Figure 3. Latitudinal cross-section of stratospheric fraction (SF) anomalies (%) averaged over 70°–85°E, on Day 0 for cyclones (a) Aila, (b) Vardah, (c) Phailin, and (d) Gonu. The dotted black vertical line shows the cyclone location. The solid black line is the dynamical tropopause (defined using the 2 PVU potential vorticity contour). The dashed gray and solid green contours show potential temperature (K) and wind speed (ms^{-1}), respectively.

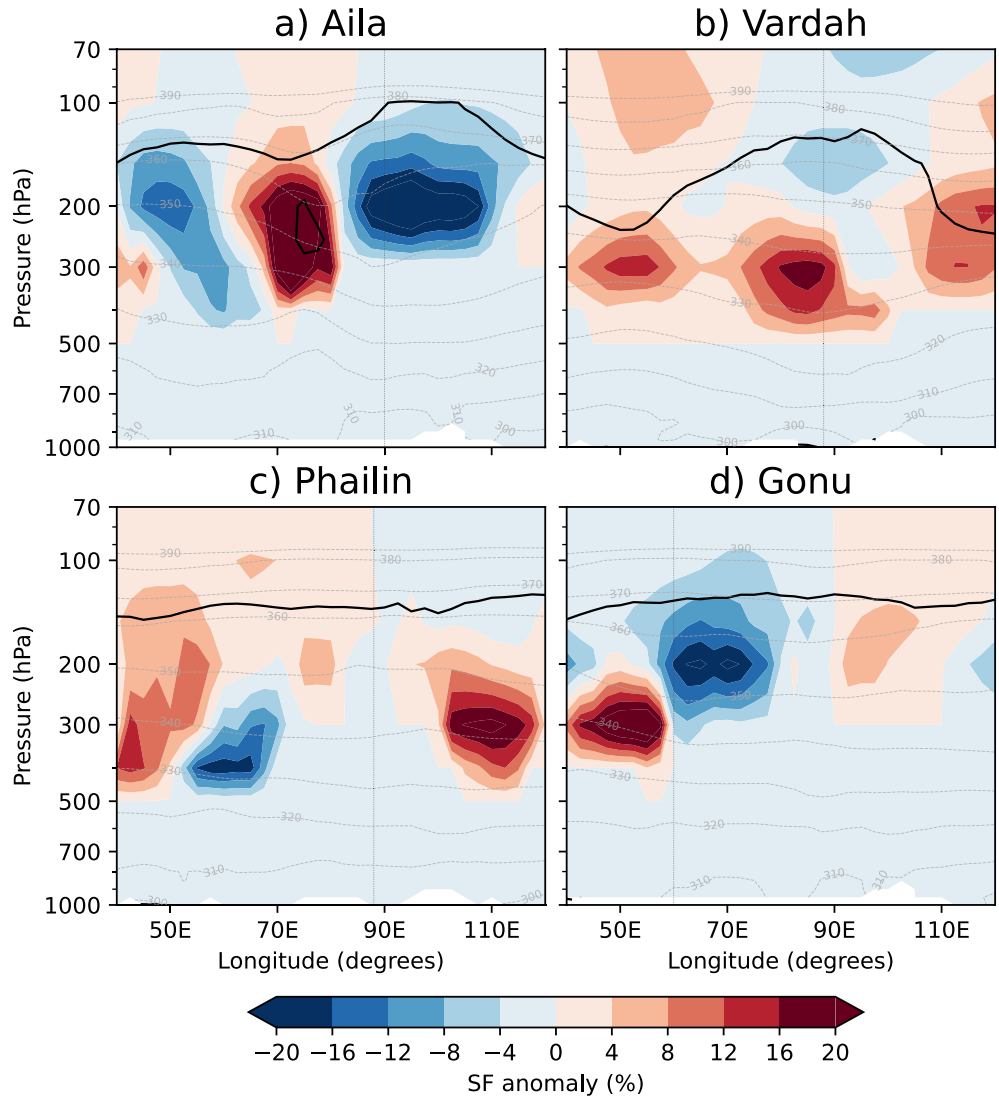

Figure 4. Longitudinal cross-section of stratospheric fraction (SF) anomalies (%) averaged over 20°–35°N on Day 0 for cyclones (a) Aila, (b) Vardah, (c) Phailin, and (d) Gonu. The dotted black vertical line shows the cyclone location. The solid black line is the dynamical tropopause (defined using the 2 PVU potential vorticity contour). The dashed gray contours show potential temperature (K).

mass exchanges across the tropopause (Hirschberg & Fritsch, 1993). An upward tropopause fold indicates the influence of deep convection associated with the NIO cyclones, whereas a downward tropopause fold (reaching 200 hPa along with positive SF) indicates the influence of stratospheric intrusion. Elevated upper tropospheric SF over India suggests that these regions may have higher-than-usual ozone concentrations.

We compare the vertical profiles of SF anomalies with the vertical profiles of ozone anomalies obtained from IAGOS aircraft measurements over different locations in India. The anomalies were calculated from the difference between the value at each level and the mean value for all the levels up to 200 hPa. Figure 5 shows the vertical profiles of ozone and SF anomalies during different cyclones. High ozone anomalies (10–50 ppb) in the mid-to-upper troposphere (600–300 hPa) near different airports roughly collocated with high SF anomalies at similar altitudes (~10%–40%). This data shows that stratospheric intrusion during the NIO cyclones contributes to upper tropospheric ozone enhancement. High ozone and low relative humidity associated with mid-latitudinal cyclone-driven tropopause fold have been previously reported from IAGOS observations (Brioude et al., 2006). IAGOS observations near typhoons near Taiwan have also been reported to have high PV, high ozone, and low CO (Roux et al., 2020). It should be mentioned here that different studies based on observations have also highlighted

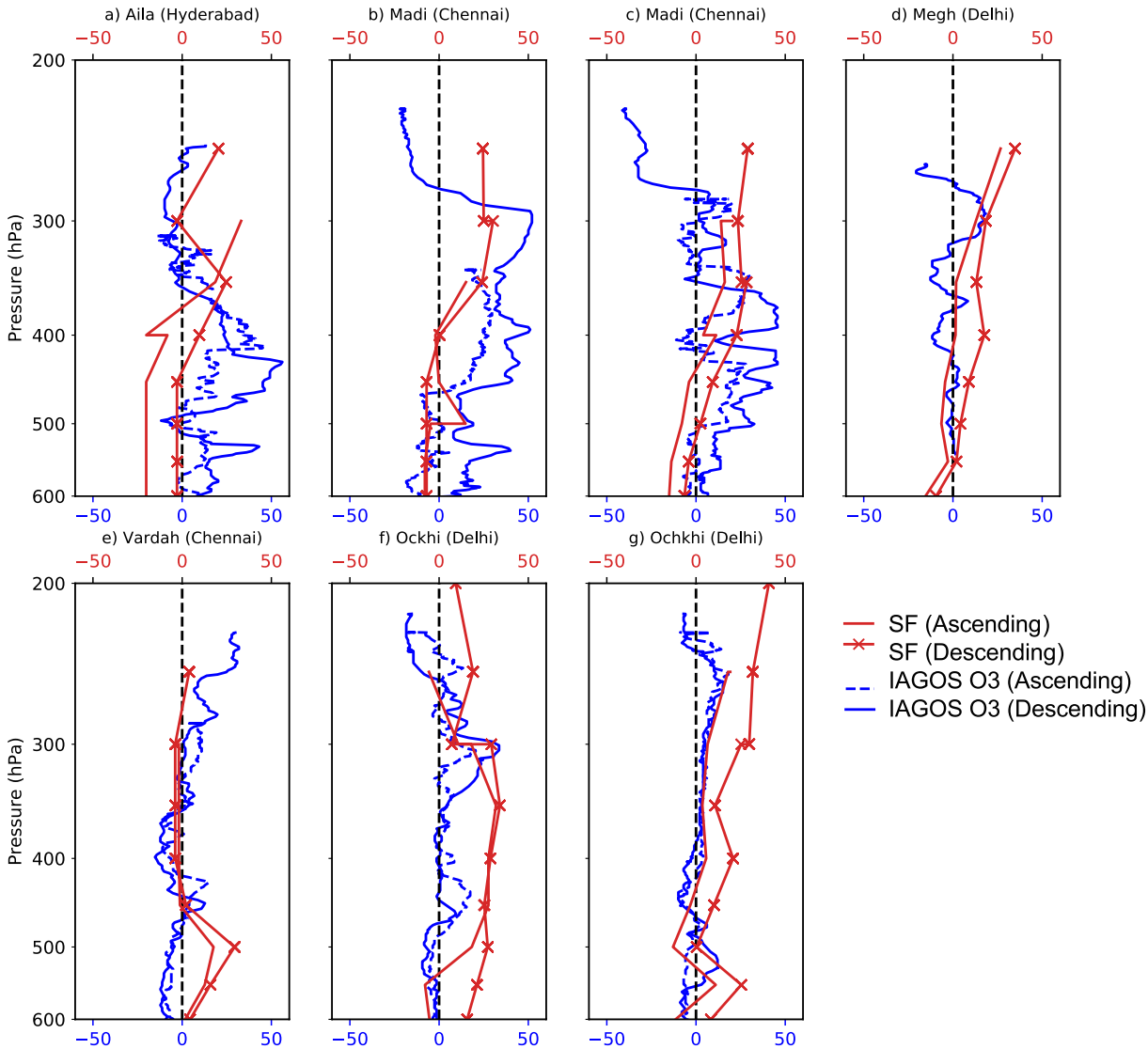

Figure 5. Vertical profiles (ascending and descending) of In-service Aircraft for a Global Observing System (IAGOS) ozone anomaly (ppb; Blue) and stratospheric fraction (SF) anomaly (%; Red) near different airports in India on or close to Day 0. SFs only for the days that coincided with the date of observations were calculated.

the role of vertically propagating waves or disturbances during tropical cyclones in causing STE (Das, 2009; Das et al., 2016b; Hocking et al., 2007; Niranjan Kumar & Ramkumar, 2008; Pathakoti et al., 2016). Waves triggered by orography, like the Himalayas, can also lead to oscillations in the wind flow and reach the upper atmosphere (Kaifler et al., 2015; Lyapustin et al., 2014; Niranjan Kumar et al., 2012). Such orography-induced waves can lead to STE and ozone enhancement over the Himalayas (K. N. Kumar et al., 2020; Phanikumar et al., 2017). Upper tropospheric ozone enhancement over India during tropical cyclones via stratospheric intrusions has been studied earlier (Das et al., 2011; Das et al., 2016a; Das et al., 2016b).

3.3. Dynamical Signatures of Stratospheric Intrusion

Dynamical exchange of airmass across the tropopause can enhance the upper tropospheric ozone concentration; downward transport of this ozone can also lead to the chemical production of additional ozone. Tropopause folds, or RWB, are dynamical phenomena that can lead to an exchange of air between the stratosphere and the troposphere (Baray et al., 1998; Folkins & Appenzeller, 1996; Gouget et al., 1996; Postel & Hitchman, 1999). They lead to the intrusions of the lower stratospheric dry, ozone-rich, and high PV air masses into the tropical upper troposphere (Konopka et al., 2010; Ploeger et al., 2012; Waugh, 2005). PV is relatively conserved under an adiabatic flow and hence is considered an ideal diagnostic for understanding the dynamical exchange of atmospheric

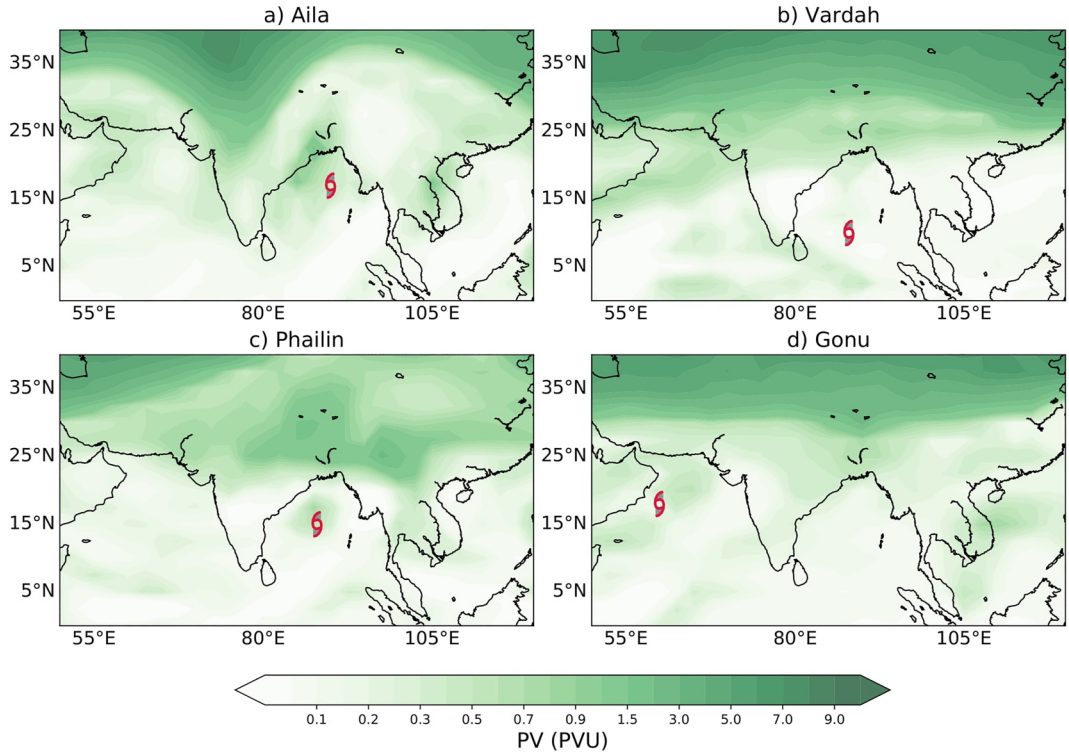

Figure 6. The distribution of 350 K PV (PVU) on Day 0 for cyclones (a) Aila, (b) Vardah, (c) Phailin, and (d) Gonu. The red markers show cyclone locations.

air parcels (Homeyer & Bowman, 2013). High PV values (>0.5 PVU) indicate stratospheric air (Roux et al., 2020; Roy et al., 2020) with a typical PV and ozone correlation near the tropopause (Browell et al., 1987). We use PV to characterize the presence of stratospheric air. Figure 6 illustrates the ERA-Interim PV at 350 K isentropic level on Day 0 for four cyclones. Use of the more recent, higher resolution, ERA5 or MERRA2 reanalysis does not change the PV location and magnitude as shown in Figure S13 in Supporting Information S1. The ERA-Interim PV at 350 K for other cyclones included in this study are shown in Figure S14 in Supporting Information S1. A strong PV gradient, similar to SF, is observed with relatively high values (>0.7 PVU) over northern India (above 15°N).

3.4. Chemical Signatures of Stratospheric Intrusion

GEOS-Chem simulated 200 hPa ozone illustrates a meridional gradient over India for four NIO cyclones (Figure S15 in Supporting Information S1) during which ozone levels were modeled. Overall, ozone was higher over northern India than in southern India. This meridional gradient in ozone is similar to that observed in the SF distribution shown in Figure S7 in Supporting Information S1. The 200 hPa MERRA2 ozone used to compute SF are also well captured by the GEOS-Chem during the cyclones, although the ozone values are slightly underestimated in GEOS-Chem (Figure S16 in Supporting Information S1). The GEOS-Chem simulated 200 hPa ozone also agrees well with the CAMS 200 hPa ozone for the NIO cyclones (Figures S15 and S17 in Supporting Information S1). Therefore we use the CAMS reanalysis data set to study the chemical signatures of stratospheric intrusion (ozone and stratospheric ozone tracer). CAMS data sets are available for all the NIO cyclones between 2007 and 2017.

Figure 7 shows the spatial distribution of CAMS 200 hPa ozone anomalies for four NIO cyclones noted in the figure. The ozone anomalies for other cyclones included in this study are shown in Figure S18 in Supporting Information S1. The ozone anomalies follow a similar distribution as SF anomalies. Regions having high ozone anomalies (~20–60 ppb) were coherent with regions having high SF anomalies (as would be expected).

Over 90 ppb of ozone is observed near the tropopause and beyond 400 hPa (Figures S19 and S20 in Supporting Information S1). Further, the ozone abundances decreased as we reached the surface. Extra-tropical exchange of ozone anomalies across the tropopause is apparent in the latitudinal cross-section of ozone anomalies.

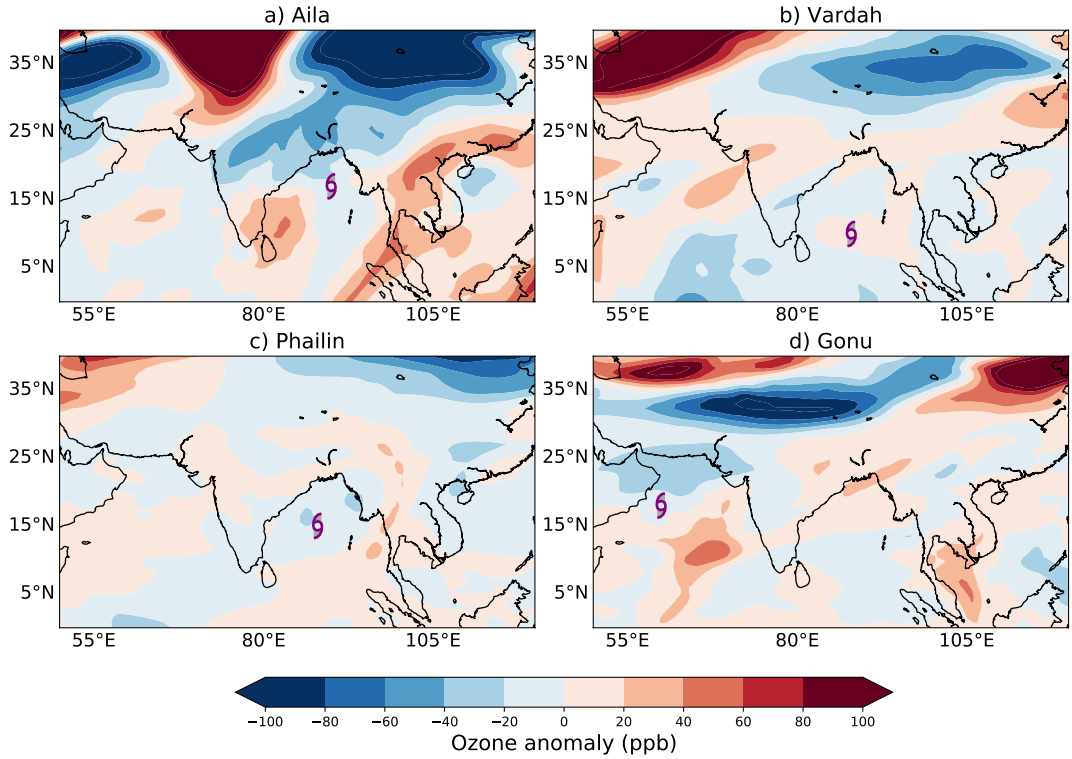

Figure 7. The distribution of 200 hPa ozone anomalies (ppb) on Day 0 for cyclones (a) Aila, (b) Vardah, (c) Phailin, and (d) Gonu. The purple markers show cyclone locations.

Figure 8 shows the latitudinal cross-section of ozone anomalies for four cyclones noted in the figure. Latitudinal cross-section of ozone anomalies for rest of the cyclones are shown in Figure S21 in Supporting Information S1. High ozone anomalies (~10–30 ppb) are observed across the tropopause, with some extensions downward to ~400 hPa. Meridional cross-tropopause ozone flux exchange has been reported to show a strong connection with the jet stream (Yang et al., 2016). We also observe the cross-tropopause exchange of high ozone anomalies in the jet stream's vicinity. Further, in many cases, this exchange allows the stratospheric ozone to intersect the ground along the low isentropic surfaces.

The longitudinal cross-sections of ozone anomalies indicate distinct tropopause folding primarily over ~70°E, highlighting the pathway of stratospheric ozone into the troposphere (Figure 9 and Figure S22 in Supporting Information S1). High SF has already been observed to intrude along the same path (Figure 4). Mid-to-upper tropospheric ozone anomalies reach ~30–50 ppb. High amounts of ozone in many cases make their way into the boundary layer, thereby elevating the surface ozone concentration by ~16 ppb. However, other processes like advection or photochemical production could also contribute to this boundary layer ozone anomalies.

Another way to look for stratospheric air other than water vapor is via examining modeled artificial tracers. We use a stratospheric ozone tracer to understand the stratospheric contribution to upper tropospheric ozone amplification. A tagging method (David & Ravishankara, 2019; Y. Zhang et al., 2012), where the tracer represents stratospheric ozone, is employed in GEOS-Chem. During four cyclone cases, the average GEOS-Chem simulated 200 hPa stratospheric ozone tracer concentrations over India were ~50 ppb (Figure S23 in Supporting Information S1). The values agree well with the CAMS stratospheric ozone tracer values (Figure S24 in Supporting Information S1). The CAMS 200 hPa stratospheric ozone tracer anomalies were high (~20–30 ppb) over northern India during ~80% of the NIO cyclones (Figure 10 and Figure S25 in Supporting Information S1).

3.5. Cyclone-Centric Composites of Measures of Stratospheric Intrusion

Figures 11a–11c show cyclone-centric composites of 200 hPa SF, 350 K PV, and 200 hPa ozone, on Day 0, for all the NIO cyclones listed in Table 1. The cyclone-centric composites were obtained in the following way. The location of each cyclone on Day 0 was first identified based on the MSLP. The variables were then extracted on

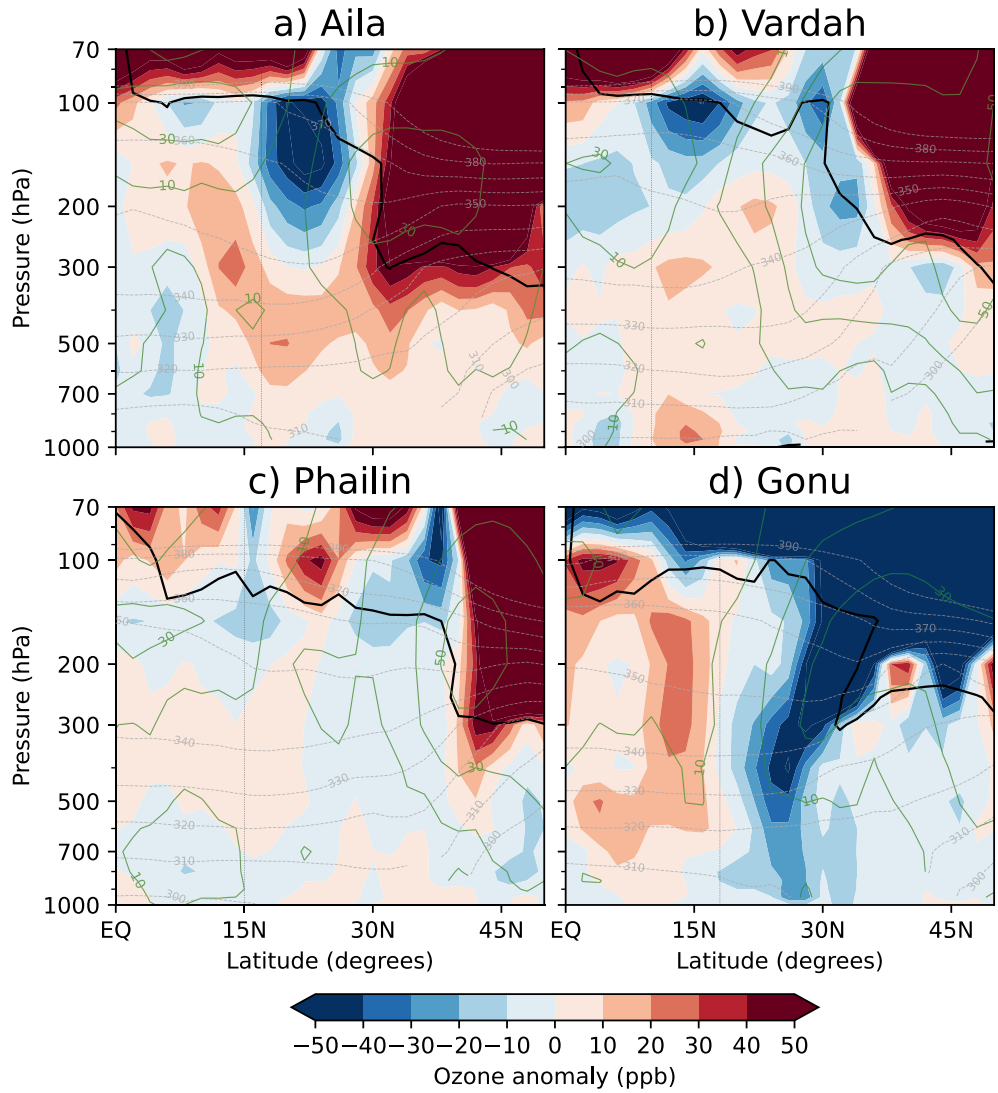

Figure 8. Latitudinal cross-section of ozone anomalies (ppb) averaged over 70°–85°E on Day 0 for cyclones (a) Aila, (b) Vardah, (c) Phailin, and (d) Gonu. The dotted black vertical line shows the cyclone location. The solid black line is the dynamical tropopause (defined using the *2* PVU potential vorticity contour). The dashed gray and solid green contours show potential temperature (K) and wind speed (ms^{-1}), respectively.

a 40° (latitude) × 40° (longitude) grid centered on the cyclone locations and then averaged together. Relatively low SF (<15%) and ozone (<70 ppb) are generally found at the cyclone center, indicating tropospheric influence (Figures 11a and 11c). Relatively high SF (>20%) and ozone (>80 ppb) observed at ∼10° east and west of the cyclone center indicate the stratospheric influence that resulted from isentropic transport or tropopause folding up to ∼200–300 hPa during >90% cyclones (seen in Figures 3, 4, 8, and 9). Simultaneously, high PV (>0.3 PVU) at the cyclone center is associated with the strong cyclonic flow of the cyclone (Figure 11b). Previous case studies have also associated convection during tropical cyclones with stratospheric intrusion (Baray et al., 1999; Loring et al., 1996), resulting in an upper tropospheric ozone enhancement near the cyclone center (Cairo et al., 2008; Leclair De Bellevue et al., 2006; Loring et al., 1996).

Cyclone-centric composites of 200 hPa ozone anomalies and their statistical significance (estimated from the Student's *t* test) for the AS and the BoB cyclones were computed to evaluate the individual influence of each basin on STE-driven ozone in the upper troposphere (Figure 12). The influence of the AS cyclones (western side of India) over the Indian landmass can be observed in the northeast (NE) and southeast (SE) quadrants. In contrast, the influence of the BoB cyclones (eastern side of India) on the Indian landmass can be observed in the northwest (NW) and southwest (SW) quadrants. The AS cyclones show high ozone anomalies primarily in the SE and SW

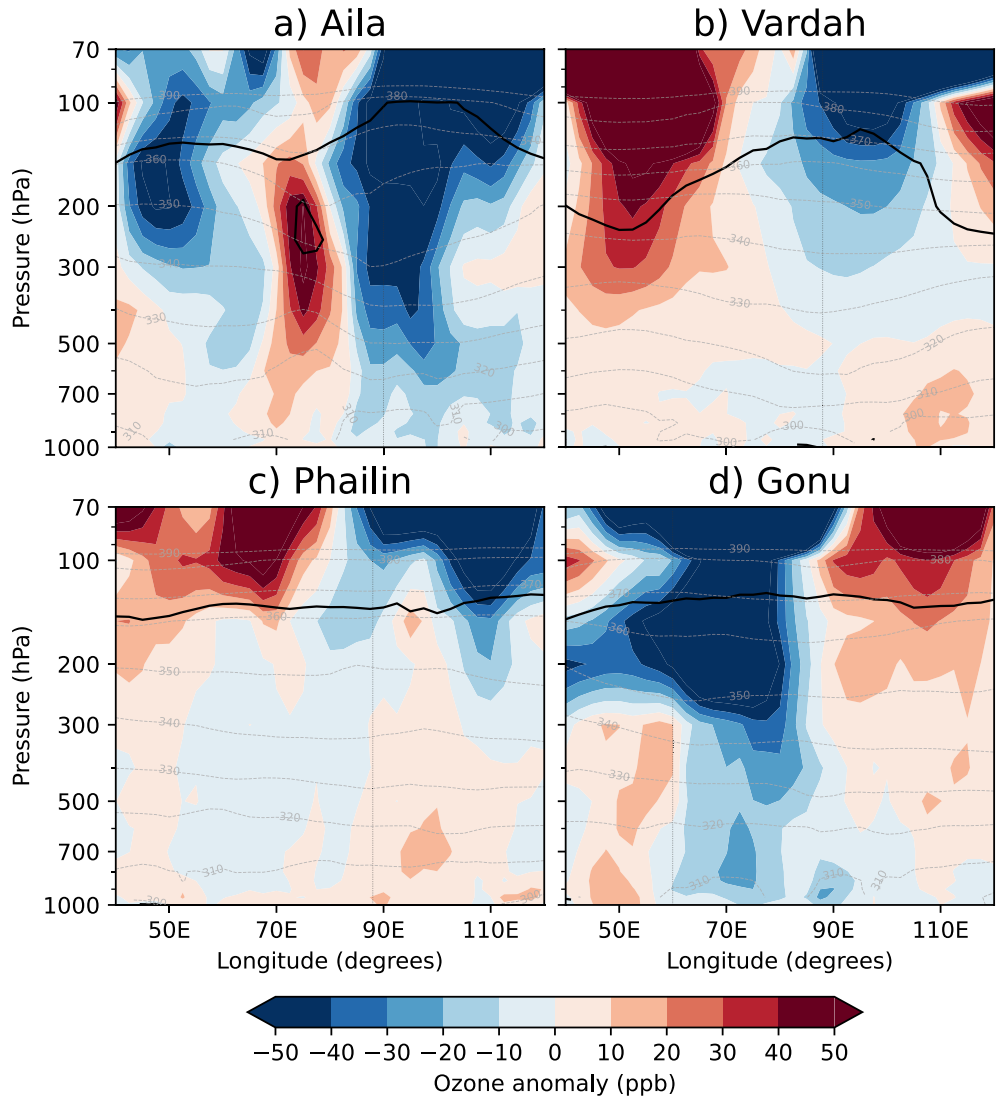

Figure 9. Longitudinal cross-section of ozone anomalies (ppb) averaged over 20°–35°N on Day 0 for cyclones (a) Aila, (b) Vardah, (c) Phailin, and (d) Gonu. The dotted black line shows the cyclone location. The solid black line is the dynamical tropopause (defined using the 2 PVU potential vorticity contour). The dashed gray contours show potential temperature (K).

quadrants, of which the SE quadrant (central-to-southern Indian region) shows statistically significant values at a 95% level (estimated from student's *t* test; Figure 12a). On the other hand, the BoB cyclones show high ozone anomalies in the SE, SW, and NW quadrants. Of these, the NW (northern-to-central Indian region) and the SE (the oceanic region near South-East Asia) quadrants show statistically significant values at 95% level, and the SW (central-to-southern India region) quadrant show statistically significant values at 85% level (Figure 12b). The negative ozone anomaly (statistically significant at 85% level), primarily in the NE quadrant, indicates the cyclone's maximum tropospheric updraft and outflow region. We observe that the AS cyclones-driven STE has more impact on central-to-southern India, whereas the BoB cyclones-driven STE has more impact on northern India. Also, stronger ozone anomalies are observed during cyclones over the AS than over the BoB. These differences may be due to various factors like the cyclones' strength and location, and the number of cyclones formed over each of these basins during our study period. In addition to these factors, it should also be noted that the six cyclones formed over the AS were all above category 3. On the other hand, of the 14 cyclones formed over the BoB, one-third of cyclones were of category 2, which could lower the mean ozone anomaly. The values of the ozone anomalies show ~50% reduction as we move from 200 to 600 hPa (Figures S26a–S26b in Supporting

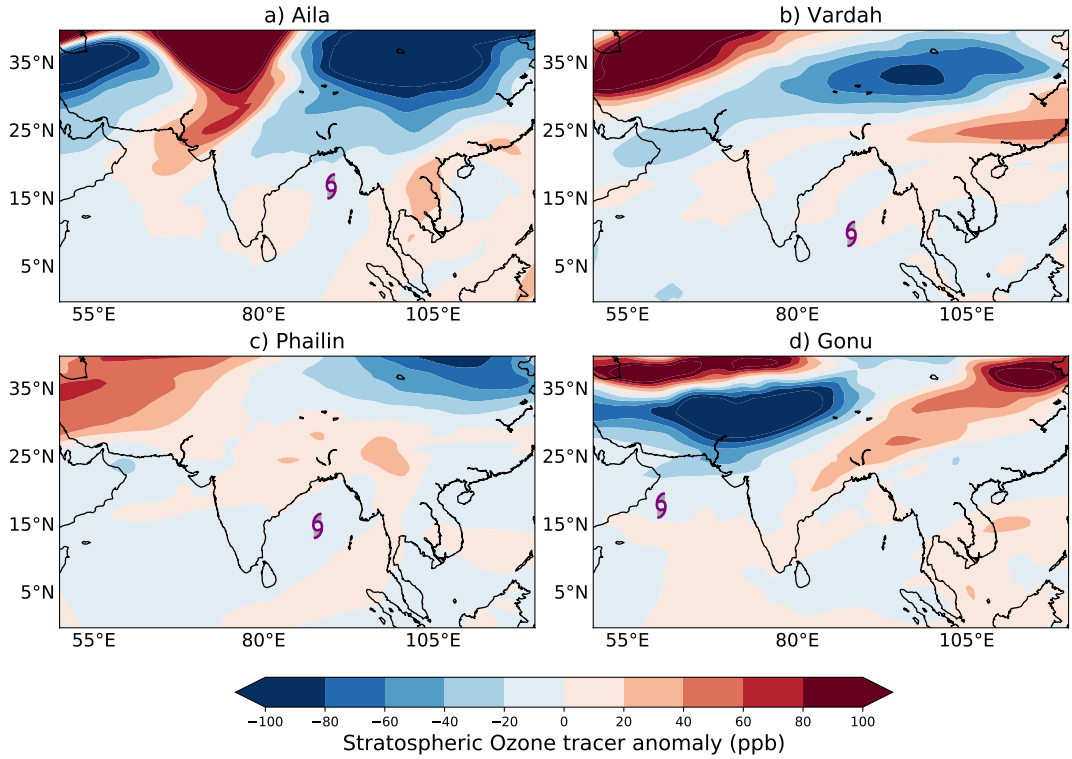

Figure 10. The distribution of 200 hPa stratospheric ozone tracer anomalies (ppb) on Day 0 for cyclones (a) Aila, (b) Vardah, (c) Phailin, and (d) Gonu. The purple markers show cyclone locations.

Information S1). Near the surface (800 hPa), the ozone anomalies are primarily influenced by photochemical production and loss of ozone (Figures S26c–S26d in Supporting Information S1).

4. Discussion

We investigate the upper-tropospheric STE induced by the NIO cyclones. The two warm NIO basins of the BoB and AS are in the tropics. Earlier studies have reported that the impacts of cyclone-driven STE are seen in the vicinity of the cyclone center (Ray & Rosenlof, 2007; Reutter et al., 2015; Venkat Ratnam et al., 2016). The NIO cyclones follow a north-westerly track and curve either southwest or northeast. Along its path, the associated deep convection disturbs the tropopause resulting in STE over India.

Observations and model simulations show the structure of cyclone-driven STE. The lack of sufficient vertical profile soundings of ozone in the vicinity of the NIO cyclones limits the use of in situ profiles to study ozone

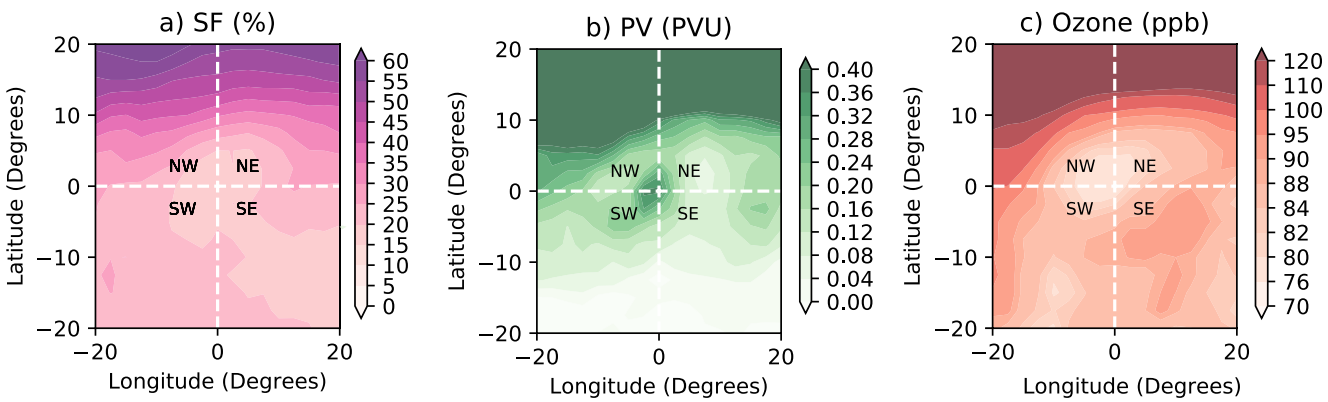

Figure 11. Cyclone-centric composites of (a) 200 hPa stratospheric fraction (SF) (%), (b) 350 K PV (PVU), and (c) 200 hPa ozone (ppb) on Day 0. The intersection of the white dashed lines indicates the average cyclone location. The four quadrants—northeast (NE), northwest (NW), southwest (SW), and southeast (SE) are marked.

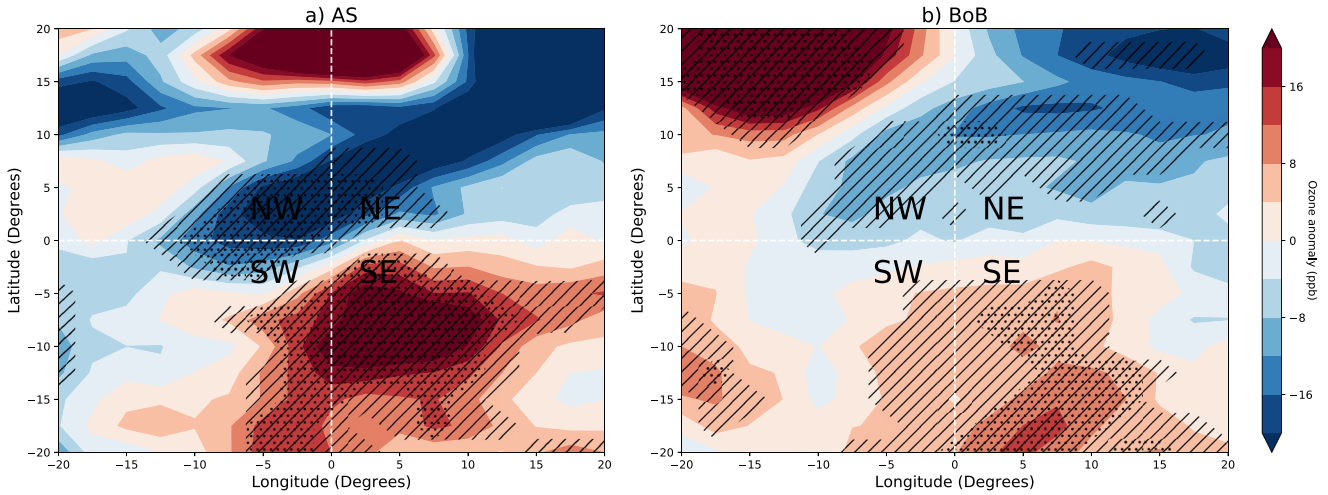

Figure 12. Cyclone-centric composites of 200 hPa ozone anomalies (ppb) on Day 0 for the (a) AS cyclones and (b) BoB cyclones. The intersection of the white dashed lines indicates the average cyclone location. The black dots and the black hatches indicate significance at 95% and 85%, respectively, calculated using Student's *t* test. The four quadrants—northeast (NE), northwest (NW), southwest (SW), and southeast (SE) are marked.

enhancements due to STE. We used (a) SF, derived from MERRA-2 ozone mixing ratios and specific humidity, (b) PV, obtained from ECMWF-Interim reanalysis, (c) ozone mixing ratios, and (d) stratospheric ozone tracer, both obtained from CAMS reanalysis and GEOS-Chem simulations to study cyclone-driven STE. While SF and ozone mixing ratios were the chemical indicators of the stratospheric air mass, PV was a dynamical indicator. The stratospheric indicators were enhanced over the Indian region, indicating stratospheric intrusion induced by the NIO cyclones.

PV and SF, obtained from reanalysis data, can be considered semi-quantitative measures of stratospheric intrusion. Over 40% SF was observed in the mid-to-upper troposphere (~200–400 hPa) over northern India, whereas less than 20% SF was observed over southern India. Relatively high PV was observed over north India, indicating the presence of stratospheric air in the upper troposphere. Since PV and ozone are correlated near the tropopause, one may quantify the contribution of ozone also from the dynamical tracers.

The vertical ozone profiles obtained from aircraft observations (IAGOS) for a few NIO cyclones showed high ozone anomalies between ~300 and 100 hPa. The aircraft profiles were sporadic and not always coincident in space and time with the NIO cyclones. However, analysis of the ozone profiles available at different Indian airports roughly capture the ozone enhancements during the NIO cyclones. The ozone enhancements were collocated with the SF enhancements obtained from reanalyses. Regions with more than 30 ppb ozone anomalies also showed more than 20% SF anomalies. CAMS and GEOS-Chem simulated 200 hPa ozone anomalies of more than 30 ppb over northern India while less than 20 ppb over southern India. The high 200 hPa stratospheric ozone model tracer anomalies (~20–30 ppb) indicated that the stratosphere contributed ~60%–70% of the upper tropospheric ozone. Although stratospheric intrusion was considered the primary factor for the increased upper tropospheric ozone, other processes like advection and photochemical production could have also contributed. However, the influence of stratospheric intrusion decreased with altitude.

The contribution of the AS cyclones (west of India) and the BoB cyclones (east of India) on ozone enhancement was more pronounced over central-southern India and northern India, respectively. This difference could be due to various factors such as the cyclone location, cyclone strength, and the number of cyclones formed over each basin (Reutter et al., 2015; Venkat Ratnam et al., 2016). The BoB cyclone activity has been reported to be four-fold higher than that of the AS (Alam et al., 2003). Stronger ocean-atmosphere coupling (high SST and moisture content) over the BoB makes it more conducive for the genesis of cyclones (Dube et al., 2009; Sahoo & Bhaskaran, 2016; Singh et al., 2001). Cyclones formed over the AS and the BoB also experience a difference in orography. The cyclones above 15°N experience a higher orography, whereas those below 15°N experience a lower orography. Tropospheric ozone enhancement from tropopause folding due to orography-induced waves generated from wind flow over the Himalayan region has also been reported earlier (Niranjan Kumar et al., 2012; Phanikumar et al., 2017). The cumulative effect of the Himalayas in northern India (25°–40°N and 70°–100°E)

and an NIO cyclone can lead to more intense stratospheric intrusion; such an analysis is beyond the scope of this study. Thus, both land and oceanic processes can influence STE during the NIO cyclones.

During 2007–2017, the most intense NIO cyclones developed during post-monsoon (October–November) or pre-monsoon (March–June) seasons. Downward propagation of ozone due to STE over India has been primarily observed during winter (December–February) and pre-monsoon (May–June). It has also been reported that dynamical processes, like RWB, during the Asian Summer monsoon also affect STE (Fadnavis & Chattopadhyay, 2017; Roy et al., 2020; Samanta et al., 2016). In this study, we primarily focus on the pre- and post-monsoon seasons, when other processes do not lead to significant STE. Therefore, the cyclones-driven STE is a dominant source of upper tropospheric ozone enhancement when we usually do not expect the classic STE via tropopause folds along the jet stream. Exchange of airmass along the isentropic surfaces results in deep intrusion of stratospheric ozone. We note that there were indications of ozone intrusions into the planetary boundary layer (up to 16 ppb), which can alter the surface ozone levels. Such excursions influence air quality.

5. Conclusion

Our study shows that the NIO cyclones significantly induce STE over India. We observe that deep convection associated with the NIO cyclones has sufficiently low CTTs, which disturbs the tropopause and leads to STE via tropopause folding and isentropic transport. As a result, enhanced values of various indicators of stratospheric intrusion like SF, PV, ozone mixing ratios, and stratospheric ozone tracer were evident in the UTLS. We also observe that the BoB cyclones have a greater influence on the ozone amplification over northern India. In comparison, the AS cyclones have a greater influence over southern India. Further, it was seen that stratospheric ozone intrusion during the NIO cyclones often reached the surface, which can have implications on air quality.

With more and stronger NIO cyclones in a warming world (Deshpande et al., 2021; Singh et al., 2001), stratospheric ozone in the troposphere could increase in the future. The high spatio-temporal resolution required to study the impacts of stratospheric intrusion during the NIO cyclones on tropospheric ozone and the limitations in corresponding in situ and satellite observations, elucidates the need for more ozonesondes launches and aircraft campaigns across various Indian locations.

Acknowledgments
C.R. and S.F. thank the Director, Indian Institute of Tropical Meteorology (IITM), for his support. IITM is funded by the Ministry of Earth Sciences (MoES) Government of India. This work is a part of the lead author's Ph.D. thesis at Savitribai Phule Pune University (SPPU). Part of this research was carried out at the Department of Atmospheric Science, Colorado State University (CSU), Fort Collins, USA under the Fulbright-Kalam Fellowship for Doctoral Research. C.R. is also thankful to Prof. J. R. Pierce, Prof. M. M. Bell, and Dr. K. R. Bilsback of CSU, and Dr. I. A. Girach of Space Physics Laboratory (SPL), India, for their helpful discussions. The authors acknowledge all data providers (ERA-Interim, MODIS, IAGOS, MERRA-2, and CAMS), whose data sets were extensively used for this study. IAGOS has been funded by the European Union projects IAGOS-Design Study (IAGOS-DS) and IAGOS-European Research Infrastructure (IAGOS-ERI). The IAGOS database is supported in France by AERIS (https://www.aeris-data.fr). The authors acknowledge the strong support of the European Commission, Airbus and the airlines (Deutsche Lufthansa, Air France, Cathay Pacific, Iberia, China Airlines and Hawaiian Airlines) that carry the IAGOS equipment.

Data Availability Statement

MODIS data used for the study is publicly available at: https://giovanni.gsfc.nasa.gov/giovanni/ (last accessed on 15 November 2022). The IAGOS, MERRA2, CAMS and ERA-Interim data sets used in this study are publicly available at: https://iagos.aeris-data.fr/, https://disc.gsfc.nasa.gov/datasets/M2I3NPASM_5.12.4/summary?keywords=merra2, https://ads.atmosphere.copernicus.eu/#/home, and https://apps.ecmwf.int/datasets/data/interim-full-daily/levtype=sfc/ (all last accessed on 15 November 2022). GEOS-Chem simulations output is available at Zenodo (https://doi.org/10.5281/zenodo.7267890).

References

Alam, M. M., Hossain, M. A., & Shafee, S. (2003). Frequency of Bay of Bengal cyclonic storms and depressions crossing different coastal zones. *International Journal of Climatology: A Journal of the Royal Meteorological Society*, *23*(9), 1119–1125. https://doi.org/10.1002/joc.927

Appenzeller, C., & Davies, H. C. (1992). Structure of stratospheric intrusions into the troposphere. *Nature*, *358*(6387), 570–572. https://doi.org/10.1038/358570a0

Appenzeller, C., Holton, J. R., & Rosenlof, K. H. (1996). Seasonal variation of mass transport across the tropopause. *Journal of Geophysical Research: Atmospheres*, *101*(D10), 15071–15078. https://doi.org/10.1029/96JD00821

Baray, J. L., Ancellet, G., Randriambelo, T., & Baldy, S. (1999). Tropical cyclone Marlene and stratosphere-troposphere exchange. *Journal of Geophysical Research: Atmospheres*, *104*(D11), 13953–13970. https://doi.org/10.1029/1999JD900028

Baray, J. L., Ancellet, G., Taupin, F. G., Bessafi, M., Baldy, S., & Keckhut, P. (1998). Subtropical tropopause break as a possible stratospheric source of ozone in the tropical troposphere. *Journal of Atmospheric and Solar-Terrestrial Physics*, *60*(1), 27–36. https://doi.org/10.1016/S1364-6826(97)00116-8

Bhutto, A. Q., Iqbal, M. J., & Baig, M. J. (2017). Abrupt intensification and dissipation of tropical cyclones in Indian Ocean: A case study of tropical cyclone Nilofar—2014. *Journal of Basic & Applied Sciences*, *13*, 566–576. https://doi.org/10.6000/1927-5129.2017.13.92

Boeke, R. C., Allan, A. M., & Coakley, J. A., Jr. (2016). Properties of marine stratocumulus obtained with partly cloudy pixel retrievals and found in the MODIS MOD06 cloud product. *Journal of Geophysical Research: Atmospheres*, *121*(11), 6404–6424. https://doi.org/10.1002/2015jd024149

Brewer, A. W. (1949). Evidence for a world circulation provided by the measurements of helium and water vapor distribution in the stratosphere. *Quarterly Journal of the Royal Meteorological Society*, *75*(326), 351–363. https://doi.org/10.1002/qj.49707532603

Brioude, J., Cammas, J. P., & Cooper, O. R. (2006). Stratosphere-troposphere exchange in a summertime extratropical low: Analysis. *Atmospheric Chemistry and Physics*, *6*(8), 2337–2353. https://doi.org/10.5194/acp-6-2337-2006

Browell, E. V., Danielsen, E. F., Ismail, S., Gregory, G. L., & Beck, S. M. (1987). Tropopause fold structure determined from airborne lidar and in situ measurements. *Journal of Geophysical Research: Atmospheres*, *92*(D2), 2112–2120. https://doi.org/10.1029/jd092id02p02112

Cairo, F., Buontempo, C., MacKenzie, A. R., Schiller, C., Volk, C. M., Adriani, A., et al. (2008). Morphology of the tropopause layer and lower stratosphere above a tropical cyclone: A case study on cyclone Davina (1999). *Atmospheric Chemistry and Physics*, *8*(13), 3411–3426. https://doi.org/10.5194/acp-8-3411-2008

Danielsen, E. F. (1993). In situ evidence of rapid, vertical, irreversible transport of lower tropospheric air into the lower tropical stratosphere by convective cloud turrets and by larger-scale upwelling in tropical cyclones. *Journal of Geophysical Research: Atmospheres*, *98*(D5), 8665–8681. https://doi.org/10.1029/92jd02954

Das, S. S. (2009). A new perspective on MST radar observations of stratospheric intrusions into-troposphere associated with tropical cyclone. *Geophysical Research Letters*, *36*(15). https://doi.org/10.1029/2009GL039184

Das, S. S., Sijikumar, S., & Uma, K. N. (2011). Further investigation on stratospheric air intrusion into the troposphere during the episode of tropical cyclone: Numerical simulation and MST radar observations. *Atmospheric Research*, *101*(4), 928–937. https://doi.org/10.1016/j.atmosres.2011.05.023

Das, S. S., Venkat Ratnam, M., Uma, K. N., Patra, A. K., Subrahmanyam, K. V., Girach, I. A., et al. (2016b). Stratospheric intrusion into the troposphere during the tropical cyclone Nilam (2012). *Quarterly Journal of the Royal Meteorological Society*, *142*(698), 2168–2179. https://doi.org/10.1002/qj.2810

Das, S. S., Venkat Ratnam, M., Uma, K. N., Subrahmanyam, K. V., Girach, I. A., Patra, A. K., et al. (2016a). Influence of tropical cyclones on tropospheric ozone: Possible implications. *Atmospheric Chemistry and Physics*, *16*(8), 4837–4847. https://doi.org/10.5194/acp-16-4837-2016

David, L. M., & Ravishankara, A. R. (2019). Boundary layer ozone across the Indian subcontinent: Who influences whom? *Geophysical Research Letters*, *46*(16), 10008–10014. https://doi.org/10.1029/2019GL082416

David, L. M., Ravishankara, A. R., Brewer, J. F., Sauvage, B., Thouret, V., Venkataramani, S., & Sinha, V. (2019). Tropospheric ozone over the Indian subcontinent from 2000 to 2015: Data set and simulation using GEOS-Chem chemical transport model. *Atmospheric Environment*, *219*, 117039. https://doi.org/10.1016/j.atmosenv.2019.117039

Dee, D. P., Uppala, S. M., Simmons, A. J., Berrisford, P., Poli, P., Kobayashi, S., et al. (2011). The ERA-Interim reanalysis: Configuration and performance of the data assimilation system. *Quarterly Journal of the Royal Meteorological Society*, *137*(656), 553–597. https://doi.org/10.1002/qj.828

Derber, J. C., Parrish, D. F., & Lord, S. J. (1991). The new global operational analysis system at the National Meteorological Center. *Weather and Forecasting*, *6*(4), 538–547. https://doi.org/10.1175/1520-0434(1991)006<0538:tngoas>2.0.co;2

Deshpande, M., Singh, V. K., Ganadhi, M. K., Roxy, M. K., Emmanuel, R., & Kumar, U. (2021). Changing status of tropical cyclones over the North Indian Ocean. *Climate Dynamics*, *57*(11), 3545–3567. https://doi.org/10.1007/s00382-021-05880-z

Dube, S. K., Jain, I., Rao, A. D., & Murty, T. S. (2009). Storm surge modeling for the Bay of Bengal and Arabian Sea. *Natural Hazards*, *51*(1), 3–27. https://doi.org/10.1007/s11069-009-9397-9

Dvorak, V. F. (1975). Tropical cyclone intensity analysis and forecasting from satellite imagery. *Monthly Weather Review*, *103*(5), 420–430. https://doi.org/10.1175/1520-0493(1975)103<0420:tciaaf>2.0.co;2

Eastham, S. D., Weisenstein, D. K., & Barrett, S. R. (2014). Development and evaluation of the unified tropospheric-stratospheric chemistry extension (UCX) for the global chemistry-transport model GEOS-Chem. *Atmospheric Environment*, *89*, 52–63. https://doi.org/10.1016/j.atmosenv.2014.02.001

European Centre for Medium-range Weather Forecast (ECMWF). (2011). The ERA-Interim reanalysis dataset. Copernicus Climate Change Service (C3S). (accessed 15 November 2022). [Dataset]. Retrieved from https://www.ecmwf.int/en/forecasts/datasets/reanalysis-datasets/era-interim

Fadnavis, S., & Chattopadhyay, R. (2017). Linkages of subtropical stratospheric intraseasonal intrusions with Indian summer monsoon deficit rainfall. *Journal of Climate*, *30*(13), 5083–5095. https://doi.org/10.1175/jcli-d-16-0463.1

Flemming, J., Benedetti, A., Inness, A., Engelen, R. J., Jones, L., Huijnen, V., et al. (2017). The CAMS interim reanalysis of carbon monoxide, ozone, and aerosol for 2003–2015. *Atmospheric Chemistry and Physics*, *17*(3), 1945–1983. https://doi.org/10.5194/acp-17-1945-2017

Flemming, J., Huijnen, V., Arteta, J., Bechtold, P., Beljaars, A., Blechschmidt, A.-M., et al. (2015). Tropospheric chemistry in the Integrated Forecasting System of ECMWF. *Geoscientific Model Development*, *8*(4), 975–1003. https://doi.org/10.5194/gmd-8-975-2015

Folkins, I., & Appenzeller, C. (1996). Ozone and potential vorticity at the subtropical tropopause break. *Journal of Geophysical Research: Atmospheres*, *101*(D13), 18787–18792. https://doi.org/10.1029/96jd01711

Folkins, I., & Martin, R. V. (2005). The vertical structure of tropical convection and its impact on the budgets of water vapor and ozone. *Journal of the Atmospheric Sciences*, *62*(5), 1560–1573. https://doi.org/10.1175/JAS3407.1

Gelaro, R., McCarty, W., Suárez, M. J., Todling, R., Molod, A., Takacs, L., et al. (2017). The Modern-Era Retrospective Analysis for Research and Applications, Version 2 (MERRA-2). *Journal of Climate*, *30*(14), 5419–5454. https://doi.org/10.1175/jcli-d-16-0758.1

Gettelman, A., & de F Forster, P. M. (2002). A climatology of the tropical tropopause layer. *Journal of the Meteorological Society of Japan. Series II*, *80*(4B), 911–924. https://doi.org/10.2151/jmsj.80.911

Gettelman, A., Hegglin, M. I., Son, S. W., Kim, J., Fujiwara, M., Birner, T., et al. (2010). Multimodel assessment of the upper troposphere and lower stratosphere: Tropics and global trends. *Journal of Geophysical Research: Atmospheres*, *115*(20), D00M08. https://doi.org/10.1029/2009JD013638

Giglio, L., Randerson, J. T., & Van Der Werf, G. R. (2013). Analysis of daily, monthly, and annual burned area using the fourth-generation Global Fire Emissions Database (GFED4). *Journal of Geophysical Research: Biogeosciences*, *118*(1), 317–328. https://doi.org/10.1002/jgrg.20042

Global Modeling and Assimilation Office (GMAO). (2015). inst3_3d_asm_Cp: MERRA-2 3D IAU State, Meteorology Instantaneous 3-hourly (p-coord, 0.625x0.5L42), version 5.12.4 [Dataset]. Space Flight Center Distributed Active Archive Center (GSFC DAAC). https://doi.org/10.5067/QBZ6MG944HW0

Gouget, H., Cammas, J., Marenco, A., Rosset, R., & Jonquières, I. (1996). Ozone peaks associated with a subtropical tropopause fold and with the trade wind inversion: A case study from the airborne campaign TROPOZ II over the Caribbean in winter. *Journal of Geophysical Research: Atmospheres*, *101*(D20), 25979–25993. https://doi.org/10.1029/96jd01545

Gray, W. M. (1968). Global view of the origin of tropical disturbances and storms. *Monthly Weather Review*, *96*(10), 669–700. https://doi.org/10.1175/1520-0493(1968)096<0669:gvotoo>2.0.co;2

Guenther, A. B., Jiang, X., Heald, C. L., Sakulyanontvittaya, T., Duhl, T., Emmons, L. K., & Wang, X. (2012). The Model of Emissions of Gases and Aerosols from Nature version 2.1 (MEGAN2. 1): An extended and updated framework for modeling biogenic emissions. *Geoscientific Model Development*, *5*(6), 1471–1492. https://doi.org/10.5194/gmd-5-1471-2012

Hirschberg, P. A., & Fritsch, J. M. (1993). A study of the development of extratropical cyclones with an analytic model. Part I: The effects of stratospheric structure. *Journal of the Atmospheric Sciences*, *50*(2), 311–327. https://doi.org/10.1175/1520-0469(1993)050<0311:ASOTDO>2.0.CO;2

Hocking, W. K., Carey-Smith, T., Tarasick, D. W., Argall, P. S., Strong, K., Rochon, Y., et al. (2007). Detection of stratospheric ozone intrusions by windprofiler radars. *Nature*, *450*(7167), 281–284. https://doi.org/10.1038/nature06312

Hoesly, R. M., Smith, S. J., Feng, L., Klimont, Z., Janssens-Maenhout, G., Pitkanen, T., et al. (2018). Historical (1750–2014) anthropogenic emissions of reactive gases and aerosols from the Community Emissions Data System (CEDS). *Geoscientific Model Development*, *11*(1), 369–408. https://doi.org/10.5194/gmd-11-369-2018

Holton, J. R., Haynes, P. H., McIntyre, M. E., Douglass, A. R., Rood, R. B., & Pfister, L. (1995). Stratosphere-troposphere exchange. *Reviews of Geophysics*, *33*(4), 403–439. https://doi.org/10.1029/95RG02097

Homeyer, C. R., & Bowman, K. P. (2013). Rossby wave breaking and transport between the tropics and extratropics above the subtropical jet. *Journal of the Atmospheric Sciences*, *70*(2), 607–626. https://doi.org/10.1175/jas-d-12-0198.1

Hoskins, B. J., McIntyre, M. E., & Robertson, A. W. (1985). On the use and significance of isentropic potential vorticity maps. *Quarterly Journal of the Royal Meteorological Society*, *111*(470), 877–946. https://doi.org/10.1002/qj.49711147002

Inness, A., Ades, M., Agustí-Panareda, A., Barré, J., Benedictow, A., Blechschmidt, A., et al. (2019). CAMS global reanalysis (EAC4). Copernicus Atmosphere Monitoring Service (CAMS) Atmosphere Data Store (ADS). [Dataset]. (Accessed on 15-11-2022). Retrieved from https://ads.atmosphere.copernicus.eu/cdsapp#!/dataset/cams-global-reanalysis-eac4?tab=overview

In-Service Aircraft for a Global Observing System (IAGOS). (2013). Retrieved from https://iagos.aeris-data.fr/

Jiang, Y. C., Zhao, T. L., Liu, J., Xu, X. D., Tan, C. H., Cheng, X. H., et al. (2015). Why does surface ozone peak before a typhoon landing in southeast China? *Atmospheric Chemistry and Physics*, *15*(23), 13331–13338. https://doi.org/10.5194/acp-15-13331-2015

Kaifler, B., Kaifler, N., Ehard, B., Dörnbrack, A., Rapp, M., & Fritts, D. C. (2015). Influences of source conditions on mountain wave penetration into the stratosphere and mesosphere. *Geophysical Research Letters*, *42*(21), 9488–9494. https://doi.org/10.1002/2015gl066465

Kaplan, J., & DeMaria, M. (2003). Large-scale characteristics of rapidly intensifying tropical cyclones in the North Atlantic basin. *Weather and Forecasting*, *18*(6), 1093–1108. https://doi.org/10.1175/1520-0434(2003)018<1093:lcorit>2.0.co;2

Keller, C. A., Long, M. S., Yantosca, R. M., Da Silva, A. M., Pawson, S., & Jacob, D. J. (2014). HEMCO v1. 0: A versatile, ESMF-compliant component for calculating emissions in atmospheric models. *Geoscientific Model Development*, *7*(4), 1409–1417. https://doi.org/10.5194/gmd-7-1409-2014

Konopka, P., Groob, J. U., Günther, G., Ploeger, F., Pommrich, R., Müller, R., & Livesey, N. (2010). Annual cycle of ozone at and above the tropical tropopause: Observations versus simulations with the chemical Lagrangian model of the stratosphere (CLaMS). *Atmospheric Chemistry and Physics*, *10*(1), 121–132. https://doi.org/10.5194/acp-10-121-2010

Kumar, K. K. (2006). VHF radar observations of convectively generated gravity waves: Some new insights. *Geophysical Research Letters*, *33*(1). https://doi.org/10.1029/2005GL024109

Kumar, K. N., Sharma, S. K., Naja, M., & Phanikumar, D. V. (2020). A Rossby wave breaking-induced enhancement in the tropospheric ozone over the Central Himalayan region. *Atmospheric Environment*, *224*, 117356. https://doi.org/10.1016/j.atmosenv.2020.117356

Lamarque, J.-F., Langford, A. O., & Proffitt, M. H. (1996). Cross-tropopause mixing of ozone through gravity wave breaking: Observation and modeling. *Journal of Geophysical Research: Atmospheres*, *101*(D17), 22969–22976. https://doi.org/10.1029/96JD02442

Langford, A. O., Alvarez, R. J., Brioude, J., Evan, S., Iraci, L. T., Kirgis, G., et al. (2018). Coordinated profiling of stratospheric intrusions and transported pollution by the Tropospheric Ozone Lidar Network (TOLNet) and NASA Alpha Jet experiment (AJAX): Observations and comparison to HYSPLIT, RAQMS, and FLEXPART. *Atmospheric Environment*, *174*, 1–14. https://doi.org/10.1016/j.atmosenv.2017.11.031

Langford, A. O., Masters, C. D., Proffitt, M. H., Hsie, E.-Y., & Tuck, A. F. (1996). Ozone measurements in a tropopause fold associated with a cut-off low system. *Geophysical Research Letters*, *23*(18), 2501–2504. https://doi.org/10.1029/96GL02227

Leclair De Bellevue, J., Baray, J. L., Baldy, S., Ancellet, G., Diab, R., & Ravetta, F. (2007). Simulations of stratospheric to tropospheric transport during the tropical cyclone Marlene event. *Atmospheric Environment*, *41*(31), 6510–6526. https://doi.org/10.1016/j.atmosenv.2007.04.040

Leclair De Bellevue, J., Réchou, A., Baray, J.-L., Ancellet, G., & Diab, R. D. (2006). Signatures of stratosphere to troposphere transport near deep convective events in the southern subtropics. *Journal of Geophysical Research: Atmospheres*, *111*(D24), D24107. https://doi.org/10.1029/2005jd006947

Lin, M., Fiore, A. M., Cooper, O. R., Horowitz, L. W., Langford, A. O., Levy, H., et al. (2012). Springtime high surface ozone events over the Western United States: Quantifying the role of stratospheric intrusions. *Journal of Geophysical Research: Atmospheres*, *117*(19), 1–20. https://doi.org/10.1029/2012JD018151

Loring, R. O., Jr., Fuelberg, H. E., Fishman, J., Watson, M. V., & Browell, E. V. (1996). Influence of a middle-latitude cyclone on tropospheric ozone distributions during a period of TRACE A. *Journal of Geophysical Research: Atmospheres*, *101*(D19), 23941–23956. https://doi.org/10.1029/95JD03573

Luo, Z., Stephens, G. L., Emanuel, K. A., Vane, D. G., Tourville, N. D., & Haynes, J. M. (2008). On the use of CloudSat and MODIS data for estimating hurricane intensity. *IEEE Geoscience and Remote Sensing Letters*, *5*(1), 13–16. https://doi.org/10.1109/LGRS.2007.905341

Lyapustin, A., Alexander, M. J., Ott, L., Molod, A., Holben, B., Susskind, J., & Wang, Y. (2014). Observation of mountain lee waves with MODIS NIR column water vapor. *Geophysical Research Letters*, *41*(2), 710–716. https://doi.org/10.1002/2013gl058770

Merrill, R. T. (1988). Characteristics of the upper-tropospheric environmental flow around hurricanes. *Journal of the Atmospheric Sciences*, *45*(11), 1665–1677. https://doi.org/10.1175/1520-0469(1988)045<1665:cotute>2.0.co;2

Mohapatra, M., Bandyopadhyay, B. K., & Tyagi, A. (2014). Status and plans for operational tropical cyclone forecasting and warning systems in the North Indian Ocean region. In *Monitoring and prediction of tropical cyclones in the Indian Ocean and climate change* (pp. 149–168). Springer.

Molod, A., Takacs, L., Suarez, M., & Bacmeister, J. (2015). Development of the GEOS-5 atmospheric general circulation model: Evolution from MERRA to MERRA-2. *Geoscientific Model Development*, *8*(5), 1339–1356. https://doi.org/10.5194/gmd-8-1339-2015

Nédélec, P., Blot, R., Boulanger, D., Athier, G., Cousin, J.-M., Gautron, B., et al. (2015). Instrumentation on commercial aircraft for monitoring the atmospheric composition on a global scale: The IAGOS system, technical overview of ozone and carbon monoxide measurements. *Tellus B: Chemical and Physical Meteorology*, *67*(1), 27791. https://doi.org/10.3402/tellusb.v67.27791

Niranjan Kumar, K., & Ramkumar, T. K. (2008). Characteristics of inertia-gravity waves over Gadanki during the passage of a deep depression over the Bay of Bengal. *Geophysical Research Letters*, *35*(13). L13804, https://doi.org/10.1029/2008GL033937

Niranjan Kumar, K., Ramkumar, T. K., & Krishnaiah, M. (2012). Analysis of large-amplitude stratospheric mountain wave event observed from the AIRS and MLS sounders over the western Himalayan region. *Journal of Geophysical Research: Atmospheres*, *117*(D22). https://doi.org/10.1029/2011JD017410

Pathakoti, M., Sujatha, P., Srinivasa, R. K., Sai Krishna, S. V. S., Rao, P. V. N., Dutt, C. B. S., & Dadhwal, V. K. (2016). Evidence of stratosphere-troposphere exchange during severe cyclones: A case study over Bay of Bengal, India. *Geomatics, Natural Hazards and Risk*, *7*(6), 1816–1823. https://doi.org/10.1080/19475705.2016.1155502

Petzold, A., Thouret, V., Gerbig, C., Zahn, A., Brenninkmeijer, C. A. M., Gallagher, M., et al. (2015). Global-scale atmosphere monitoring by in-service aircraft-current achievements and future prospects of the European Research Infrastructure IAGOS. *Tellus B: Chemical and Physical Meteorology*, *67*(1), 28452. https://doi.org/10.3402/tellusb.v67.28452

Phanikumar, D. V., Kumar, K. N., Bhattacharjee, S., Naja, M., Girach, I. A., Nair, P. R., & Kumari, S. (2017). Unusual enhancement in tropospheric and surface ozone due to orography induced gravity waves. *Remote Sensing of Environment*, *199*, 256–264. https://doi.org/10.1016/j.rse.2017.07.011

Platnick, S., Hubanks, P., Meyer, K., & King, M. D. (2015). *MODIS Atmosphere L3 Monthly Product (08_L3)* [Dataset]. NASA MODIS Adaptive Processing System, Goddard Space Flight Center. https://doi.org/10.5067/MODIS/MOD08_M3.006 (Terra), https://doi.org/10.5067/MODIS/MYD08_M3.006 (Aqua)

Platnick, S., King, M. D., Ackerman, S. A., Menzel, W. P., Baum, B. A., Riédi, J. C., & Frey, R. A. (2003). The MODIS cloud products: Algorithms and examples from Terra. *IEEE Transactions on Geoscience and Remote Sensing*, *41*(2), 459–473. [Dataset]. https://doi.org/10.1109/tgrs.2002.808301

Ploeger, F., Konopka, P., Müller, R., Fueglistaler, S., Schmidt, T., Manners, J. C., et al. (2012). Horizontal transport affecting trace gas seasonality in the Tropical Tropopause Layer (TTL). *Journal of Geophysical Research: Atmospheres*, *117*(9), 1–16. https://doi.org/10.1029/2011JD017267

Postel, G. A., & Hitchman, M. H. (1999). A climatology of Rossby wave breaking along the subtropical tropopause. *Journal of the Atmospheric Sciences*, *56*(3), 359–373. https://doi.org/10.1175/1520-0469(1999)056<0359:acorwb>2.0.co;2

Ravindra Babu, S., Venkat Ratnam, M., Basha, G., Krishnamurthy, B. V., & Venkateswararao, B. (2015). Effect of tropical cyclones on the tropical tropopause parameters observed using COSMIC GPS RO data. *Atmospheric Chemistry and Physics*, *15*(18), 10239–10249. https://doi.org/10.5194/acp-15-10239-2015

Ray, E. A., & Rosenlof, K. H. (2007). Hydration of the upper troposphere by tropical cyclones. *Journal of Geophysical Research: Atmospheres*, *112*(12), 1–11. https://doi.org/10.1029/2006JD008009

Reutter, P., Škerlak, B., Sprenger, M., & Wernli, H. (2015). Stratosphere-troposphere exchange (STE) in the vicinity of North Atlantic cyclones. *Atmospheric Chemistry and Physics*, *15*(19), 10939–10953. https://doi.org/10.5194/acp-15-10939-2015

Riehl, H. (1950). A model of hurricane formation. *Journal of Applied Physics*, *21*(9), 917–925. https://doi.org/10.1063/1.1699784

Roelofs, G.-J., & Lelieveld, J. (1997). Model study of the influence of cross-tropopause O_3 transports on tropospheric O_3 levels. *Tellus B: Chemical and Physical Meteorology*, *49*(1), 38–55. https://doi.org/10.3402/tellusb.v49i1.15949

Romps, D. M., & Kuang, Z. (2009). Overshooting convection in tropical cyclones. *Geophysical Research Letters*, *36*(9). L09804. https://doi.org/10.1029/2009GL037396

Roux, F., Clark, H., Wang, K.-Y., Rohs, S., Sauvage, B., & Nédélec, P. (2020). The influence of typhoons on atmospheric composition deduced from IAGOS measurements over Taipei. *Atmospheric Chemistry and Physics*, *20*(6), 3945–3963. https://doi.org/10.5194/acp-20-3945-2020

Roy, C., Fadnavis, S., Müller, R., Ayantika, D. C., Ploeger, F., & Rap, A. (2017). Influence of enhanced Asian NOx emissions on ozone in the upper troposphere and lower stratosphere in chemistry-climate model simulations. *Atmospheric Chemistry and Physics*, *17*(2), 1297–1311. https://doi.org/10.5194/acp-17-1297-2017

Roy, C., Fadnavis, S., & Sabin, T. P. (2020). The stratospheric ozone rich cold intrusion during El-Niño over the Indian region: Implication during the Indian summer monsoon. *International Journal of Climatology*, *41*(S1), E233–E248. https://doi.org/10.1002/joc.6680

Sahoo, B., & Bhaskaran, P. K. (2016). Assessment on historical cyclone tracks in the Bay of Bengal, East Coast of India. *International Journal of Climatology*, *36*(1), 95–109. https://doi.org/10.1002/joc.4331

Samanta, D., Dash, M. K., Goswami, B. N., & Pandey, P. C. (2016). Extratropical anticyclonic Rossby wave breaking and Indian summer monsoon failure. *Climate Dynamics*, *46*(5–6), 1547–1562. https://doi.org/10.1007/s00382-015-2661-7

Shaji, C., Kar, S. K., & Vishal, T. (2014). Storm surge studies in the North Indian Ocean: A review. *Indian Journal of Geo-Marine Sciences*, *43*(2), 125–147.

Shapiro, M. A. (1976). The role of turbulent heat flux in the generation of potential vorticity in the vicinity of upper-level jet stream systems. *Monthly Weather Review*, *104*(7), 892–906. https://doi.org/10.1175/1520-0493(1976)104<0892:TROTHF>2.0.CO;2

Singh, O. P., Khan, T. M. A., & Rahman, M. S. (2001). Has the frequency of intense tropical cyclones increased in the North Indian Ocean? *Current Science*, 575–580.

Sprenger, M., Maspoli, M. C., & Wernli, H. (2003). Tropopause folds and cross-tropopause exchange: A global investigation based upon ECMWF analyses for the time period March 2000 to February 2001. *Journal of Geophysical Research*, *108*(D12), 8518. https://doi.org/10.1029/2002JD002587

Stohl, A. (2001). A 1 yr Lagrangian "climatology" of airstreams in the Northern Hemisphere troposphere and lowermost stratosphere. *Journal of Geophysical Research: Atmospheres*, *106*(D7), 7263–7279. https://doi.org/10.1029/2000JD900570

Thouret, V., Cammas, J. P., Sauvage, B., Athier, G., Zbinden, R., Nédélec, P., et al. (2006). Tropopause referenced ozone climatology and inter-annual variability (1994–2003) from the MOZAIC program. *Atmospheric Chemistry and Physics*, *6*(4), 1033–1051. https://doi.org/10.5194/acp-6-1033-2006

Uppala, S. M., Kållberg, P. W., Simmons, A. J., Andrae, U., da Costa Bechtold, V., Fiorino, M., et al. (2005). The ERA-40 re-analysis. *Quarterly Journal of the Royal Meteorological Society*, *131*(612), 2961–3012. https://doi.org/10.1256/qj.04.176

Velden, C., Harper, B., Wells, F., Beven, J., Zehr, R. M., Olander, T. L., et al. (2006). The Dvorak tropical cyclone intensity estimation technique: A satellite-based method that has endured for over 30 yr. *Bulletin of the American Meteorological Society*, *87*, 1195–1210.

Venkat Ratnam, M., Ravindra Babu, S., Das, S. S., Basha, G., Krishnamurthy, B. V., & Venkateswararao, B. (2016). Effect of tropical cyclones on the stratosphere-troposphere exchange observed using satellite observations over the North Indian Ocean. *Atmospheric Chemistry and Physics*, *16*(13), 8581–8591. https://doi.org/10.5194/acp-16-8581-2016

Vergados, P., Luo, Z. J., Emanuel, K., & Mannucci, A. J. (2014). Observational tests of hurricane intensity estimations using GPS radio occultations. *Journal of Geophysical Research: Atmospheres*, *119*(4), 1936–1948. https://doi.org/10.1002/2013JD020934

Voulgarakis, A., Savage, N. H., Wild, O., Braesicke, P., Young, P. J., Carver, G. D., & Pyle, J. A. (2010). Interannual variability of tropospheric composition: The influence of changes in emissions, meteorology, and clouds. *Atmospheric Chemistry and Physics*, *10*(5), 2491–2506. https://doi.org/10.5194/acp-10-2491-2010

Wargan, K., Labow, G., Frith, S., Pawson, S., Livesey, N., & Partyka, G. (2017). Evaluation of the ozone fields in NASA's MERRA-2 reanalysis. *Journal of Climate*, *30*(8), 2961–2988. https://doi.org/10.1175/jcli-d-16-0699.1

Waugh, D. W. (2005). Impact of potential vorticity intrusions on subtropical upper tropospheric humidity (Vol. *110*). https://doi.org/10.1029/2004JD005664

Wernli, H., & Bourqui, M. (2002). A Lagrangian "1 yr climatology" of (deep) cross-tropopause exchange in the extratropical Northern Hemisphere. *Journal of Geophysical Research: Atmospheres*, *107*(D2), 4021. https://doi.org/10.1029/2001JD000812

Wild, O. (2007). Modeling the global tropospheric ozone budget: Exploring the variability in current models. *Atmospheric Chemistry and Physics*, *7*(10), 2643–2660. https://doi.org/10.5194/acp-7-2643-2007

Wong, V., & Emanuel, K. (2007). Use of cloud radars and radiometers for tropical cyclone intensity estimation. *Geophysical Research Letters*, *34*(12). L12811, https://doi.org/10.1029/2007GL029960

Yang, H., Chen, G., Tang, Q., & Hess, P. (2016). Quantifying isentropic stratosphere-troposphere exchange of ozone. *Journal of Geophysical Research: Atmospheres*, *121*(7), 3372–3387. https://doi.org/10.1002/2015JD024180

Zachariasse, M., Smit, H. G. J., van Velthoven, P. F. J., & Kelder, H. (2001). Cross-tropopause and interhemispheric transports into the tropical free troposphere over the Indian Ocean. *Journal of Geophysical Research: Atmospheres*, *106*(D22), 28441–28452. https://doi.org/10.1029/2001JD900061

Zhan, R., & Wang, Y. (2012). Contribution of tropical cyclones to stratosphere-troposphere exchange over the northwest Pacific: Estimation based on AIRS satellite retrievals and ERA-Interim data. *Journal of Geophysical Research: Atmospheres*, *117*(D12). https://doi.org/10.1029/2012JD017494

Zhang, L., Lin, M., Langford, A. O., Horowitz, L. W., Senff, C. J., Klovenski, E., et al. (2020). Characterizing sources of high surface ozone events in the southwestern U.S. with intensive field measurements and two global models. *Atmospheric Chemistry and Physics*, *20*(17), 10379–10400. https://doi.org/10.5194/acp-20-10379-2020

Zhang, Y., Liu, H., Crawford, J. H., Considine, D. B., Chan, C., Oltmans, S. J., & Thouret, V. (2012). Distribution, variability and sources of tropospheric ozone over south China in spring: Intensive ozonesonde measurements at five locations and modeling analysis. *Journal of Geophysical Research: Atmospheres*, *117*(D12). https://doi.org/10.1029/2012JD017498